95 MeV/A ^{12}C fragmentation for hadrontherapy: experimental measurements and comparisons with GEANT4 simulations.

Jérémie Dudouet

Laboratoire de Physique Corpusculaire de Caen

Séminaire CEA Saclay: vendredi 31 Janvier 2014

Why Hadrontherapy ?

Cancer in France (2010 data)

- $\sim$ 355 000 new cases per year
- $\sim$ 150 000 radiotherapy (X-rays) per year

45% success

- 22% surgery
- 9% surgery + radiotherapy
- 9% radiotherapy only
- 5% chemotherapy

55% failure

- 18% local failure
- 37% metastases

Heavy ions therapies

- Hadrontherapy appears as a new treatment tool for localized and radio-resistant tumours.

The advantages of carbon ions

Very accurate dose depostion location

- Charged particles ⇒ Bragg peak
- Heavy ions ⇒ small lateral deflexion

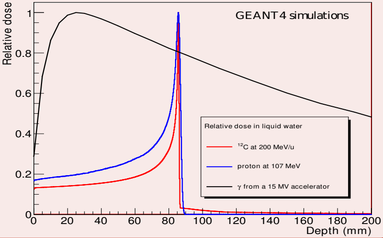

A high biological efficiency

The advantages of carbon ions

Very accurate dose depostion location

- Charged particles ⇒ Bragg peak
- Heavy ions ⇒ small lateral deflexion

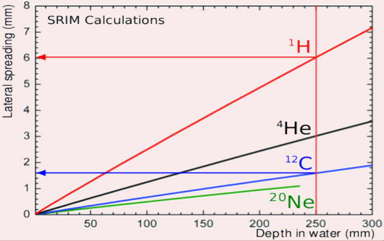

A high biological efficiency

The advantages of carbon ions

Very accurate dose depostion location

- Charged particles ⇒ Bragg peak
- Heavy ions ⇒ small lateral deflexion

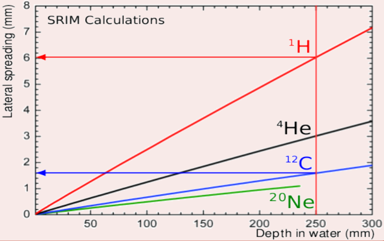

A high biological efficiency

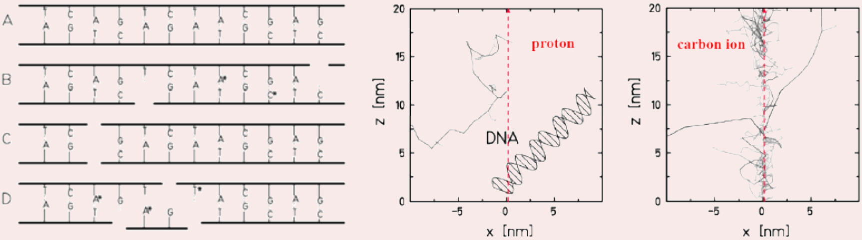

The advantages of carbon ions

Very accurate dose depostion location

- Charged particles ⇒ Bragg peak
- Heavy ions ⇒ small lateral deflexion

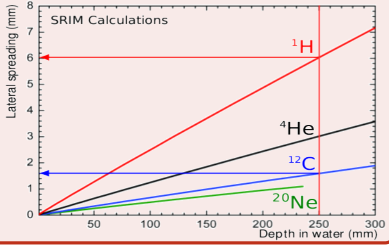

A high biological efficiency

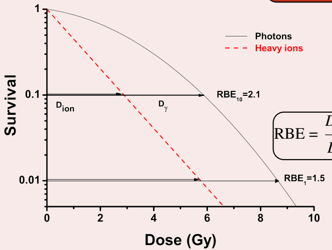

$$\mathrm{RBE} = \frac{D_{X-rays}}{D_{particle}}$$

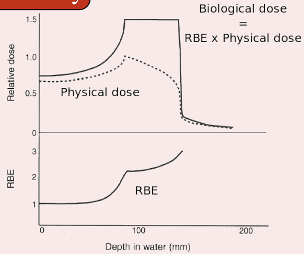

Relevance of $\frac{\partial^2\sigma}{\partial\Omega\partial E}$ fragmentation measurements

Medical impact of projectile fragmentation in ion therapy

Mixed radiation fields due to projectile fragmentation:

- LET distributions $\Rightarrow$ biological effectiveness modification,
- dose delivered: $\searrow$ inside tumor, $\nearrow$ outside tumor.

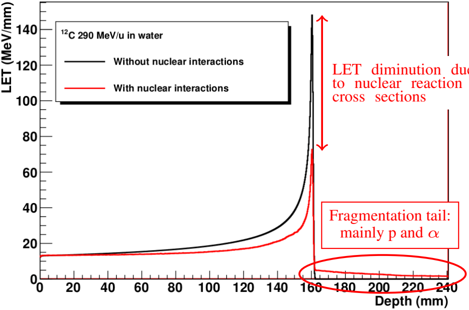

D. Cussol - LPC Caen

M. Scholz - GSI Darmstadt

Relevance of $\frac{\partial^2\sigma}{\partial\Omega\partial E}$ fragmentation measurements

Medical impact of projectile fragmentation in ion therapy

Mixed radiation fields due to projectile fragmentation:

- LET distributions $\Rightarrow$ biological effectiveness modification,
- dose delivered: $\searrow$ inside tumor, $\nearrow$ outside tumor.

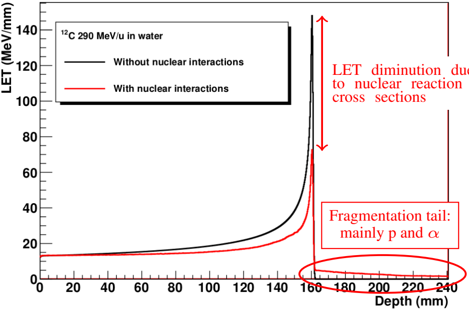

D. Cussol - LPC Caen

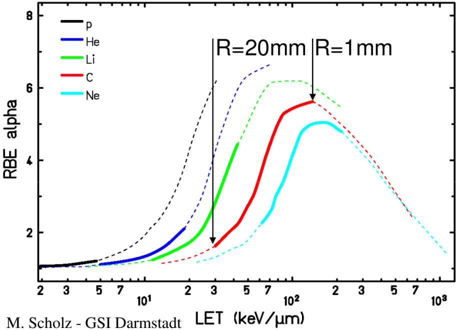

M. Scholz - GSI Darmstadt

Relevance of $\frac{\partial^2\sigma}{\partial\Omega\partial E}$ fragmentation measurements

Medical impact of projectile fragmentation in ion therapy

Mixed radiation fields due to projectile fragmentation:

- LET distributions $\Rightarrow$ biological effectiveness modification,
- dose delivered: $\searrow$ inside tumor, $\nearrow$ outside tumor.

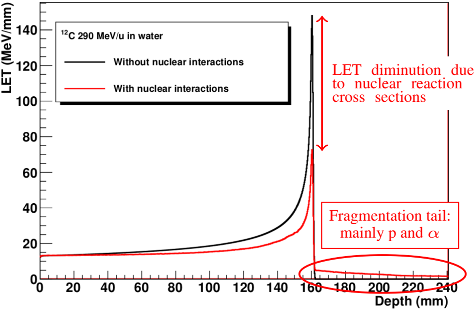

D. Cussol - LPC Caen

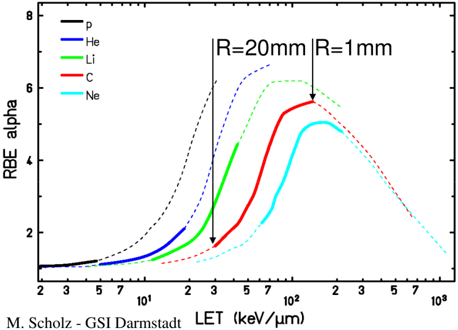

M. Scholz - GSI Darmstadt

Fragmentation has to be considered for dose calculation.

Relevance of $\frac{\partial^2\sigma}{\partial\Omega\partial E}$ fragmentation measurements

Monte Carlo codes for hadrontherapy

- Development of a reference MC code to constrain and optimize analytical treatment planning systems (TPS),
- Up to now, simulation codes do not reproduce fragmentation with the required accuracy (3% on the dose deposited inside the tumor).

$\Rightarrow$ Experimental data are needed to constrain nuclear models in the domain of energy useful for carbon-therapy (up to 400 MeV/u).

The E600 experiment at GANIL (may 2011)

- Projectile: 95 MeV/A ^{12}C
- Thin targets: C, CH_2, Al, Al_2O_3, ^{nat}Ti and PMMA ($C_5H_8O_2$)

$\Rightarrow \frac{\partial^2\sigma}{\partial\Omega\partial E}$ fragmentation measurements of ^{12}C on $\underbrace{\text{C, H, O and Ca}}_{\approx 95\% \text{ of a human body composition}}$ ($A_{Ti} \sim A_{Ca}$)

Relevance of $\frac{\partial^2\sigma}{\partial\Omega\partial E}$ fragmentation measurements

Monte Carlo codes for hadrontherapy

- Development of a reference MC code to constrain and optimize analytical treatment planning systems (TPS),
- Up to now, simulation codes do not reproduce fragmentation with the required accuracy (3% on the dose deposited inside the tumor).

$\Longrightarrow$ Experimental data are needed to constrain nuclear models in the domain of energy useful for carbon-therapy (up to 400 MeV/u).

The E600 experiment at GANIL (may 2011)

- Projectile: 95 MeV/A ^{12}C
- Thin targets: C, CH_2, Al, Al_2O_3, ^{nat}Ti and PMMA ($C_5H_8O_2$)

$\Rightarrow \frac{\partial^2\sigma}{\partial\Omega\partial E}$ fragmentation measurements of ^{12}C on $\underbrace{\text{C, H, O and Ca}}_{\approx 95\% \text{ of a human body composition}}$ ($A_{Ti} \sim A_{Ca}$)

Outlines

Cross section measurement

Cross section expression

$$\frac{d\sigma}{d\Omega}({}^{Z}_{A}X) = \frac{N_{{}^{Z}_{A}X} \times A_{target}}{N_{{}^{12}C_{inc}} \times \Omega \times \rho \times th \times \mathrm{N}_{\mathcal{A}}}$$

Setup

- Well known target: thickness(th) and density(ρ) ($\Delta(\rho \times th) \approx 1\%$)
- Charged particle telescope: isotope identification, energy and angles measurements $\Rightarrow Z, A, E, \theta, \Omega$ ($\Delta N \approx 5-10\%$, $\Delta E \approx 10\%$)
- Beam monitor $\Rightarrow N_{{}^{12}C_{inc}}$ ($\Delta N_{{}^{12}C_{inc}} \approx 5\%$)

Cross section measurement

Cross section expression

$$\frac{d\sigma}{d\Omega}({}^{Z}_{A}X) = \frac{N_{{}^{Z}_{A}X} \times A_{target}}{N_{{}^{12}C_{inc}} \times \Omega \times \rho \times th \times \mathrm{N}_{\mathcal{A}}}$$

Setup

- Well known target: thickness(th) and density(ρ) ($\Delta(\rho \times th) \approx 1\%$)
- Charged particle telescope: isotope identification, energy and angles measurements $\Rightarrow Z, A, E, \theta, \Omega$ ($\Delta N \approx 5 - 10\%$, $\Delta E \approx 10\%$)
- Beam monitor $\Rightarrow N_{{}^{12}C_{inc}}$ ($\Delta N_{{}^{12}C_{inc}} \approx 5\%$)

Cross section measurement

Cross section expression

$$\frac{d\sigma}{d\Omega}({}^{Z}_{A}X) = \frac{N_{{}^{Z}_{A}X} \times A_{target}}{N_{{}^{12}C_{inc}} \times \Omega \times \rho \times th \times \mathrm{N}_{\mathcal{A}}}$$

Setup

- Well known target: thickness(th) and density(ρ) ($\Delta(\rho \times th) \approx 1\%$)
- Charged particle telescope: isotope identification, energy and angles measurements $\Rightarrow Z, A, E, \theta, \Omega$ ($\Delta N \approx 5 - 10\%$, $\Delta E \approx 10\%$)
- Beam monitor $\Rightarrow N_{{}^{12}C_{inc}}$ ($\Delta N_{{}^{12}C_{inc}} \approx 5\%$)

Experimental setup

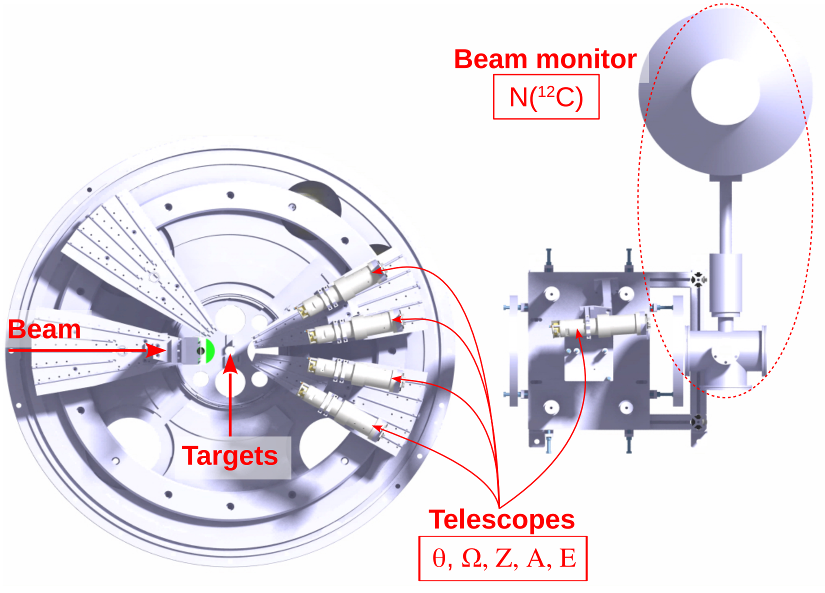

Telescope analysis: The ΔE-E method

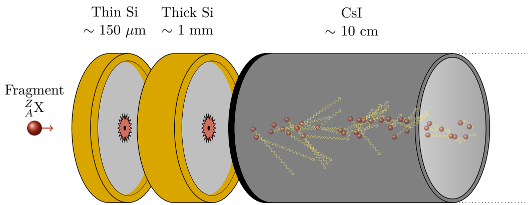

Telescope analysis: The ΔE-E method

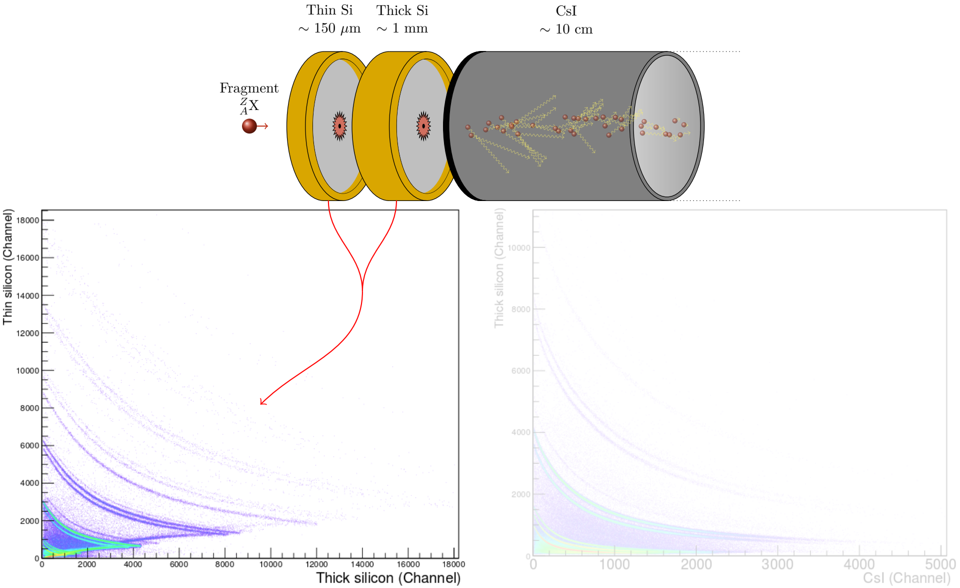

Telescope analysis: The ΔE-E method

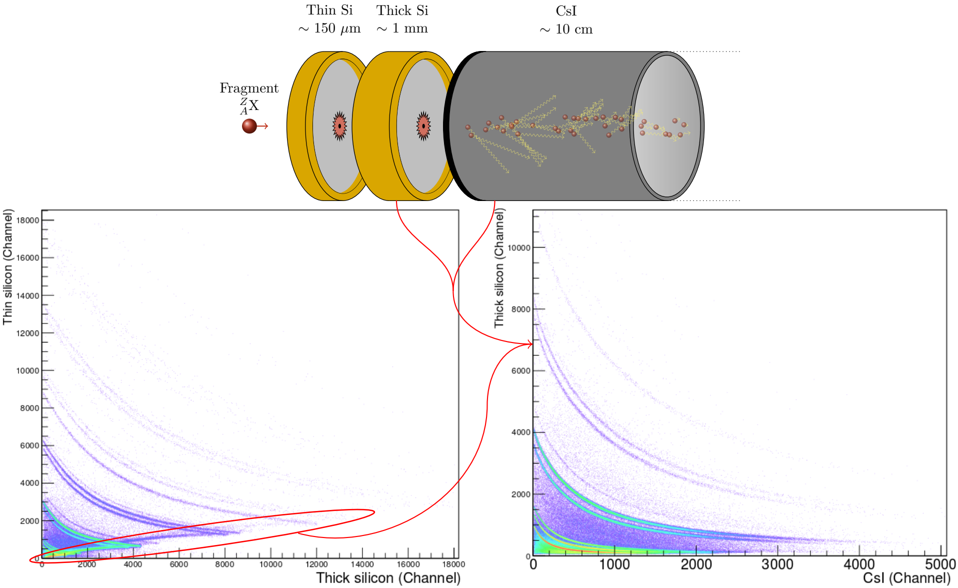

Telescope analysis: Energy calibration

- Development of an algorithm to simplify the analysis. By building an identification grid for each telescope, the algorithm will process:
  - ⇒ the energy calibration,
  - ⇒ the particle identification.

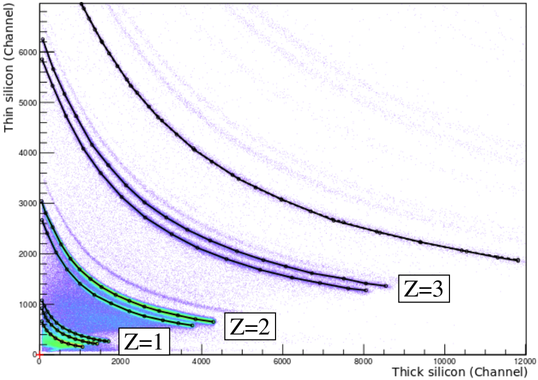

J. Dudouet *et al.*, Nucl. Instrum. Methods A 715, 98 (2013)

Telescope analysis: Energy calibration

- Development of an algorithm to simplify the analysis. By building an identification grid for each telescope, the algorithm will process:
  - ⇒ the energy calibration,
  - ⇒ the particle identification.

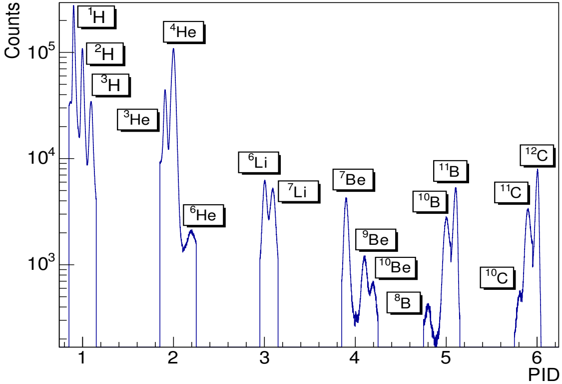

J. Dudouet *et al.*, Nucl. Instrum. Methods A 715, 98 (2013)

Outlines

Systematic errors: GEANT4 simulations

In order to estimate the systematic errors:

- GEANT4 simulations have been performed, taking into account the real experimental setup
- The simulated data have been analyzed with the same method used for the experimental data

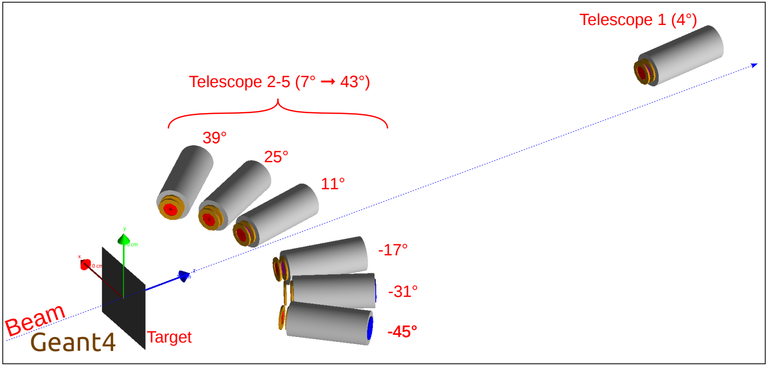

Systematic errors: GEANT4 simulations

In order to estimate the systematic errors:

- GEANT4 simulations have been performed, taking into account the real experimental setup
- The simulated data have been analyzed with the same method used for the experimental data

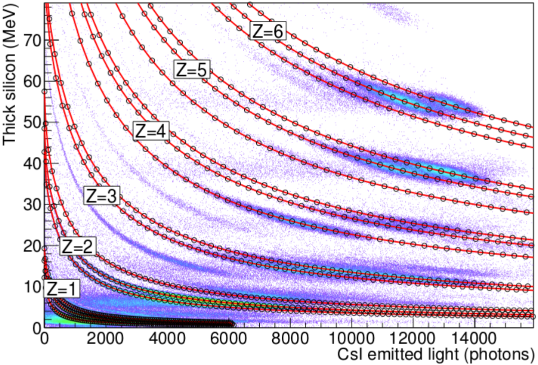

Systematic errors: GEANT4 simulations

- Two main sources of systematic errors:
  - $\Rightarrow$ Nucleus-nucleus interactions in the detectors
  - $\Rightarrow$ Pile-up of 2 α from the same event (mainly from ^{8}Be)
  - $\Rightarrow$ ^{4}He $\searrow$, ^{6}He, ^{6}Li, ^{7}Li $\nearrow$

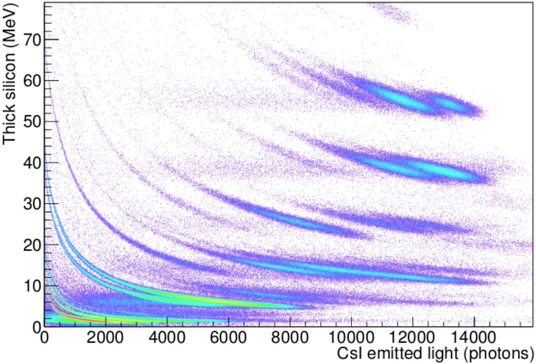

Systematic errors: GEANT4 simulations

- Two main sources of systematic errors:
  - $\Rightarrow$ Nucleus-nucleus interactions in the detectors
  - $\Rightarrow$ Pile-up of 2 α from the same event (mainly from ^{8}Be)
  - $\Rightarrow$ ^{4}He $\searrow$, ^{6}He, ^{6}Li, ^{7}Li $\nearrow$

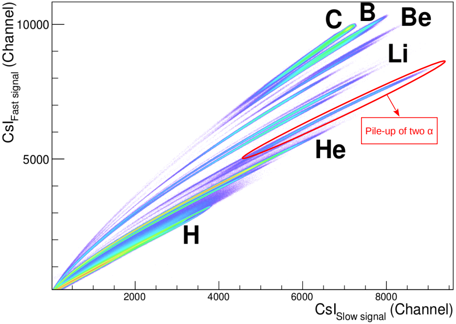

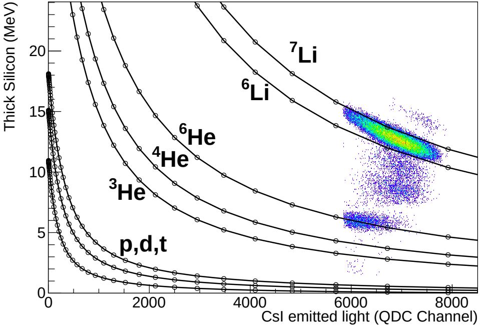

J. Dudouet *et al.*, Phys. Rev. C 88, 024606 (2013)

Systematic errors: GEANT4 simulations

- Two alpha pile-up correction:
  - ⇒ Effect validated by the simulations
  - ⇒ But corrected from the experimental pulse shape analysis (fast/slow map)

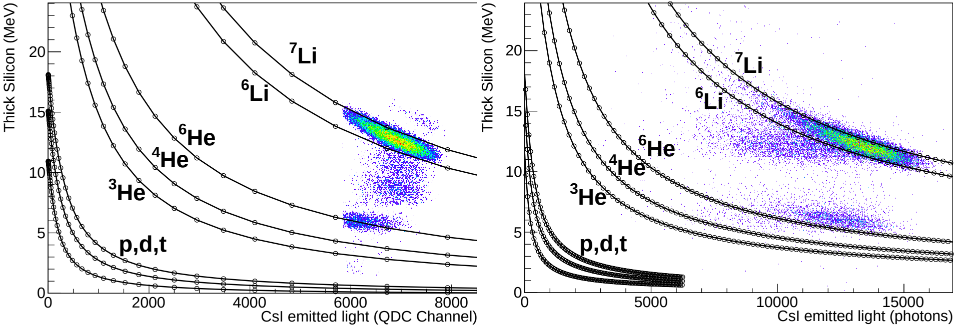

J. Dudouet *et al.*, Phys. Rev. C 88, 024606 (2013)

Systematic errors: GEANT4 simulations

- Two alpha pile-up correction:
  - ⇒ Effect validated by the simulations
  - ⇒ But corrected from the experimental pulse shape analysis (fast/slow map)

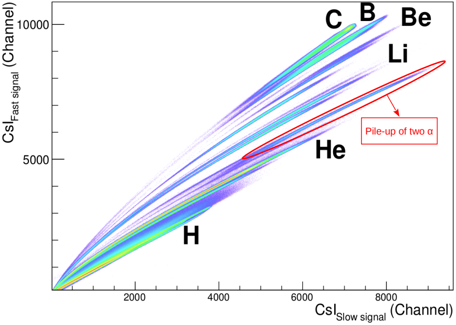

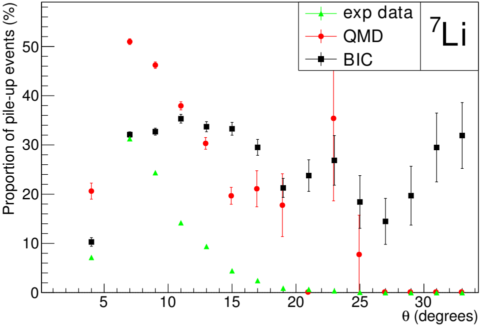

J. Dudouet *et al.*, Phys. Rev. C 88, 024606 (2013)

Systematic errors: GEANT4 simulations

- Two alpha pile-up correction:
  - ⇒ Effect validated by the simulations
  - ⇒ But corrected from the experimental pulse shape analysis (fast/slow map)

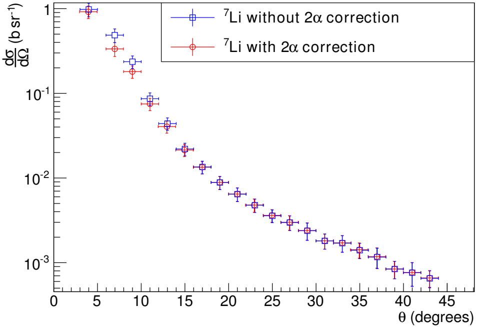

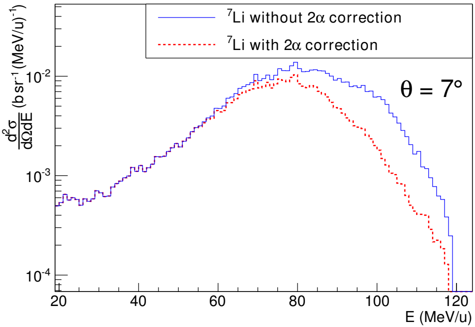

J. Dudouet *et al.*, Phys. Rev. C 88, 024606 (2013)

Systematic errors: GEANT4 simulations

- Estimation of the systematic errors:
  - ⇒ Two α pile-up: Experimental correction
  - ⇒ General case: Using simulations

$$\text{Syst Err} = 100 \times \left(1 - \frac{\mathrm{N}_{\text{Identified particles}}\left({}^{A}_{Z}\mathrm{X}\right)}{\mathrm{N}_{\text{Emitted in simulations}}\left({}^{A}_{Z}\mathrm{X}\right)}\right)$$

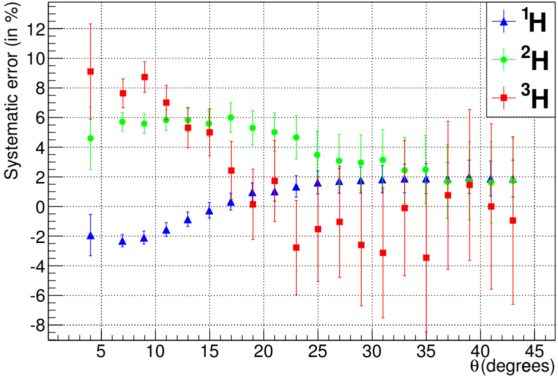

Systematic errors: GEANT4 simulations

- Estimation of the systematic errors:

  ⇒ Two α pile-up: Experimental correction

  ⇒ General case: Using simulations

$$\text{Syst Err} = 100 \times \left(1 - \frac{\mathrm{N}_{\text{Identified particles}}\left({}^{A}_{Z}\mathrm{X}\right)}{\mathrm{N}_{\text{Emitted in simulations}}\left({}^{A}_{Z}\mathrm{X}\right)}\right)$$

Systematic error estimation per isotope

Isotope ^{A}X	^{1}H	^{2}H	^{3}H	^{3}He	^{4}He	^{6}He	^{6}Li	^{7}Li
Relative error (%)	3	6	10	10	5	20	10	10

Isotope ^{A}X	^{7}Be	^{9}Be	^{10}Be	^{8}B	^{10}B	^{11}B	^{10}C	^{11}C	^{12}C
Relative error (%)	5	6	10	50	10	10	50	10	10

⇒ These systematic errors have been added in the error bars of the experimental results.

J. Dudouet *et al.*, Phys. Rev. C 88, 024606 (2013)

Outlines

The participant-spectator reaction mechanism

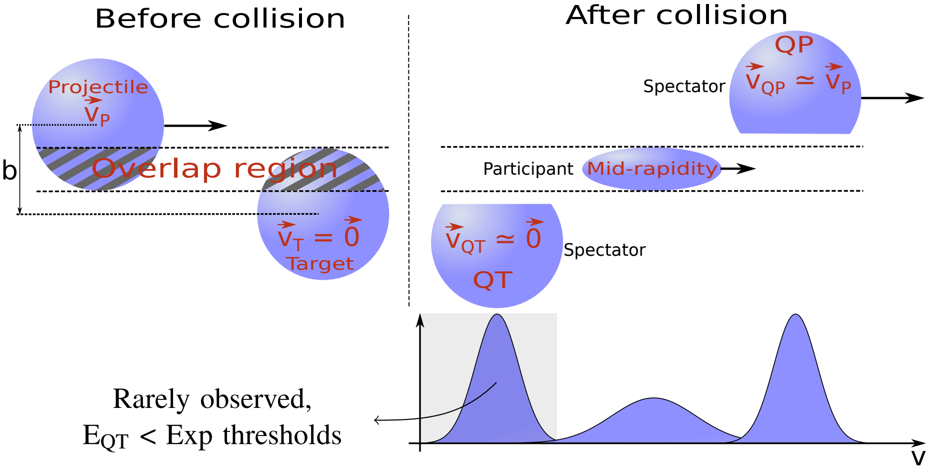

Rarely observed,
E_{QT} < Exp thresholds

Angular distributions representation & Uncertainties

Angular distributions representation

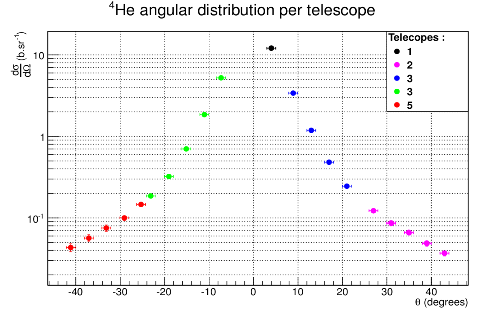

$\longrightarrow$ Measurements for $\theta \in [-41°; 43°]$

Uncertainties

- The error bars takes into account:
  - $\Rightarrow$ Statistical & systematic errors (5-10%)
  - $\Rightarrow$ Beam monitor calibration (5%)
  - $\Rightarrow$ Solid angle (2-5%)
  - $\Rightarrow$ Target area density (0.5 %)

Total error $\sim$ (7-15 %)

Angular distributions representation & Uncertainties

Angular distributions representation

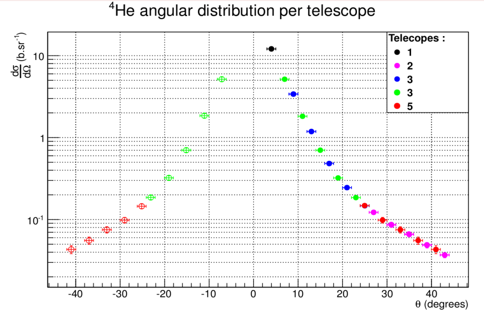

$\longrightarrow$ Measurements for $\theta \in [-41°; 43°]$

$\longrightarrow$ Representation on $\theta \in [0; 43°]$

Uncertainties

- The error bars takes into account:
  - $\Rightarrow$ Statistical & systematic errors (5-10%)
  - $\Rightarrow$ Beam monitor calibration (5%)
  - $\Rightarrow$ Solid angle (2-5%)
  - $\Rightarrow$ Target area density (0.5 %)

Total error $\sim$ (7-15 %)

Angular distributions representation & Uncertainties

Angular distributions representation

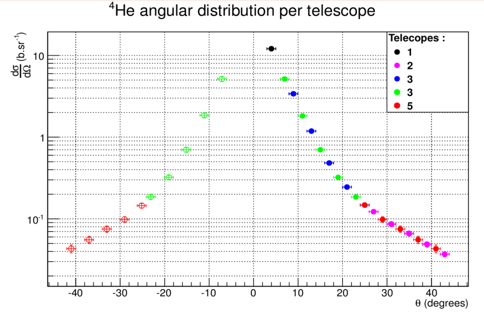

⟶ Measurements for $\theta \in [-41°; 43°]$

⟶ Representation on $\theta \in [0; 43°]$

Uncertainties

- The error bars takes into account:
  - ⇒ Statistical & systematic errors (5-10%)
  - ⇒ Beam monitor calibration (5%)
  - ⇒ Solid angle (2-5%)
  - ⇒ Target area density (0.5 %)

Total error ∼ (7-15 %)

Angular distributions for the carbon target

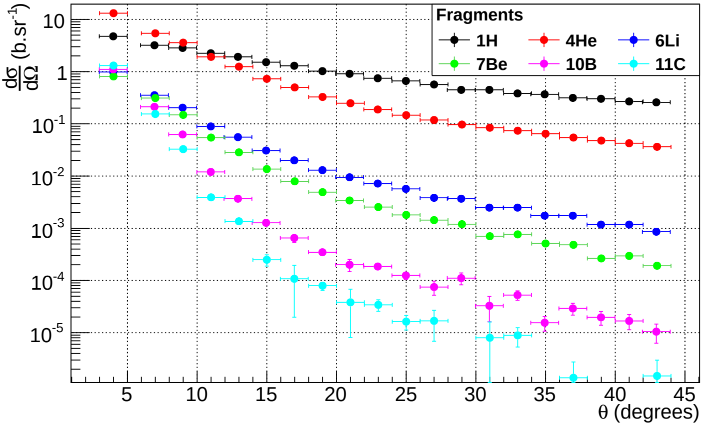

- Production is dominated by Z=1 and Z=2.
- ^{4}He production dominates below 10°.
- The heavier the fragments, the more focused at small angles.

Hydrogen and oxygen target cross sections

Cross section combination

$$\frac{d\sigma}{d\Omega}(\mathrm{O}) = \frac{1}{3} \times \left(\frac{d\sigma}{d\Omega}(\mathrm{Al_2O_3}) - 2 \times \frac{d\sigma}{d\Omega}(\mathrm{Al}) \right)$$

$$\frac{d\sigma}{d\Omega}(\mathrm{H}) = \frac{1}{2} \times \left(\frac{d\sigma}{d\Omega}(\mathrm{CH_2}) - \frac{d\sigma}{d\Omega}(\mathrm{C}) \right)$$

Hydrogen example

1. CH_2 cross sections measurement
2. Carbon cross section subtraction
3. Division by 2 to obtain Hydrogen cross sections

Hydrogen and oxygen target cross sections

Cross section combination

$$\frac{d\sigma}{d\Omega}(\mathrm{O}) = \frac{1}{3} \times \left(\frac{d\sigma}{d\Omega}(\mathrm{Al_2O_3}) - 2 \times \frac{d\sigma}{d\Omega}(\mathrm{Al}) \right)$$

$$\frac{d\sigma}{d\Omega}(\mathrm{H}) = \frac{1}{2} \times \left(\frac{d\sigma}{d\Omega}(\mathrm{CH_2}) - \frac{d\sigma}{d\Omega}(\mathrm{C}) \right)$$

Hydrogen example

1. CH_2 cross sections measurement
2. Carbon cross section subtraction
3. Division by 2 to obtain Hydrogen cross sections

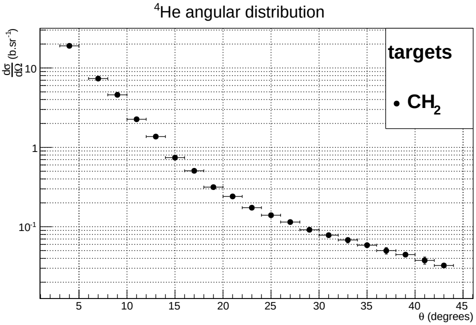

Hydrogen and oxygen target cross sections

Cross section combination

$$\frac{d\sigma}{d\Omega}(\mathrm{O}) = \frac{1}{3} \times \left(\frac{d\sigma}{d\Omega}(\mathrm{Al_2O_3}) - 2 \times \frac{d\sigma}{d\Omega}(\mathrm{Al}) \right)$$

$$\frac{d\sigma}{d\Omega}(\mathrm{H}) = \frac{1}{2} \times \left(\frac{d\sigma}{d\Omega}(\mathrm{CH_2}) - \frac{d\sigma}{d\Omega}(\mathrm{C}) \right)$$

Hydrogen example

1. CH_2 cross sections measurement
2. Carbon cross section subtraction
3. Division by 2 to obtain Hydrogen cross sections

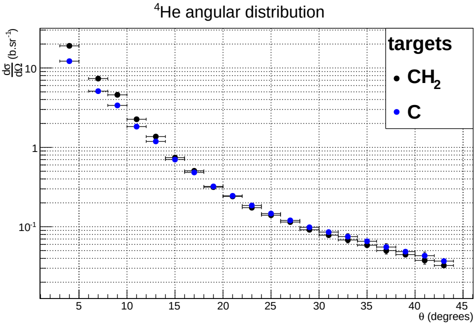

Hydrogen and oxygen target cross sections

Cross section combination

$$\frac{d\sigma}{d\Omega}(\mathrm{O}) = \frac{1}{3} \times \left(\frac{d\sigma}{d\Omega}(\mathrm{Al_2O_3}) - 2 \times \frac{d\sigma}{d\Omega}(\mathrm{Al}) \right)$$

$$\frac{d\sigma}{d\Omega}(\mathrm{H}) = \frac{1}{2} \times \left(\frac{d\sigma}{d\Omega}(\mathrm{CH_2}) - \frac{d\sigma}{d\Omega}(\mathrm{C}) \right)$$

Hydrogen example

1. CH_2 cross sections measurement
2. Carbon cross section subtraction
3. Division by 2 to obtain Hydrogen cross sections

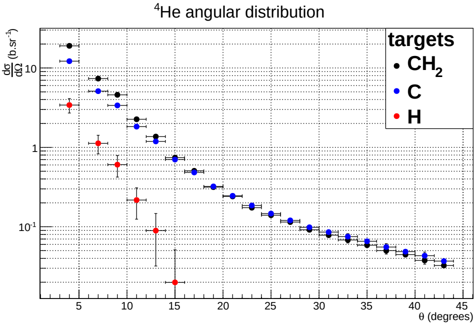

Angular distributions for all elemental targets

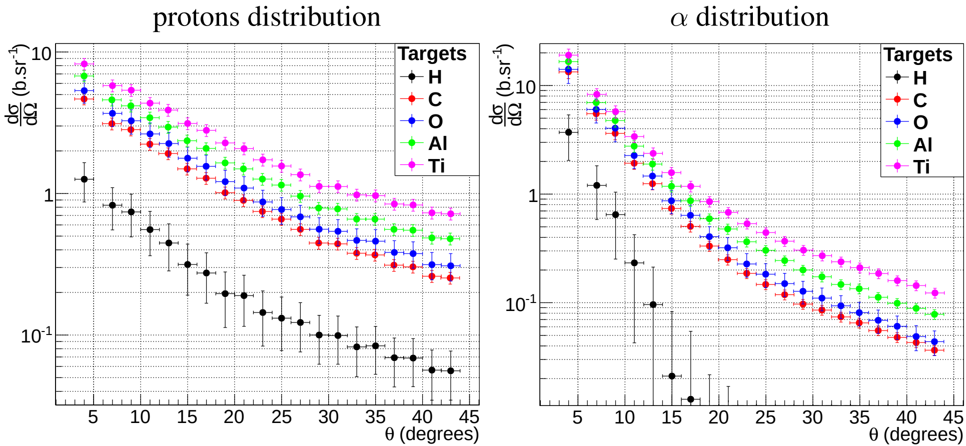

- $d\sigma/d\Omega$ increases with the target mass, especially at large angles.
- No emission of fragments heavier than Z=1 at large angles for the hydrogen target.

Angular distributions: Gaussian + Exponential fit

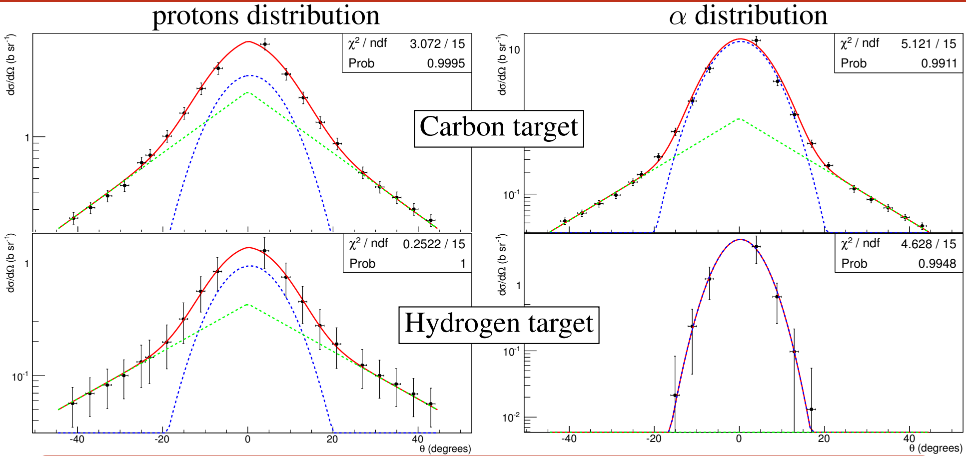

- Gaussian component at forward angle → quasi-projectile contribution
- Exponential component → mid-rapidity contribution

Angular distributions: Gaussian + Exponential fit

protons distribution | α distribution

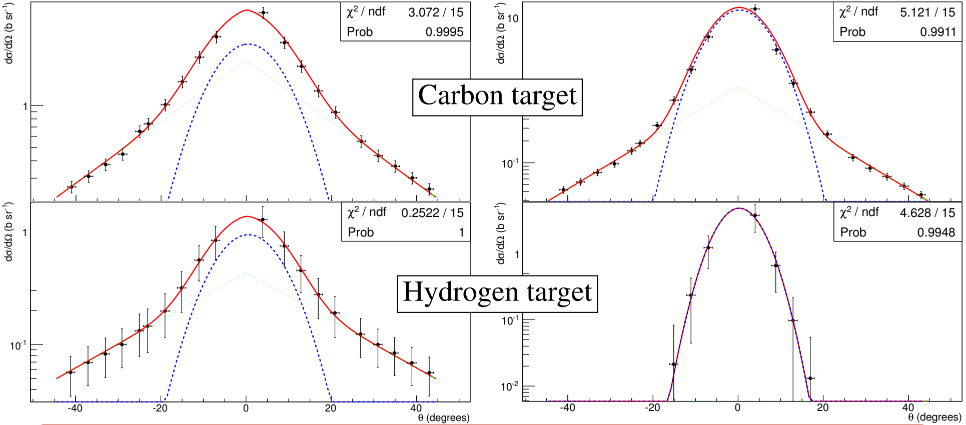

- Gaussian component at forward angle → quasi-projectile contribution
- Exponential component → mid-rapidity contribution

Angular distributions: Gaussian + Exponential fit

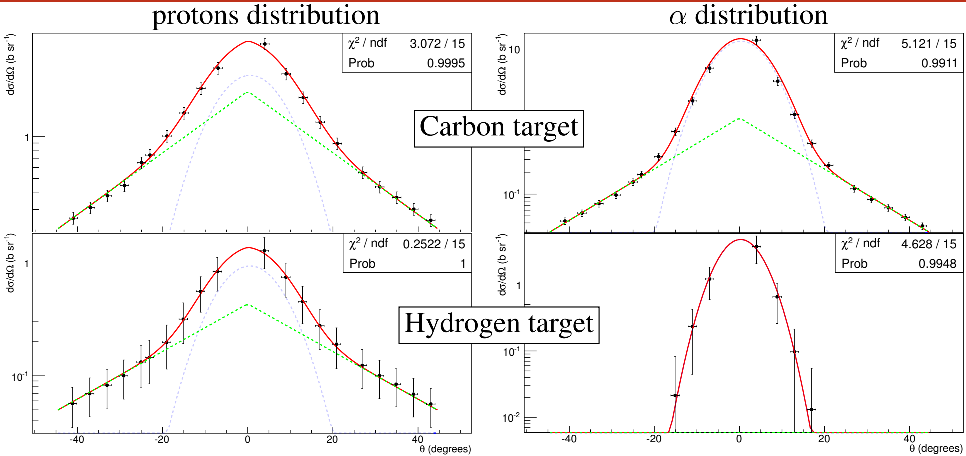

- Gaussian component at forward angle → quasi-projectile contribution
- Exponential component → mid-rapidity contribution

Angular distributions: Gaussian + Exponential fit

protons distribution α distribution

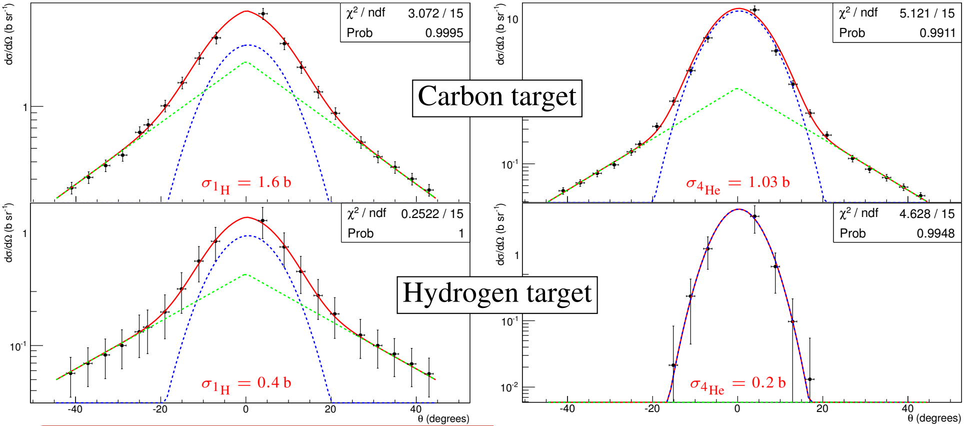

- Gaussian component at forward angle → quasi-projectile contribution
- Exponential component → mid-rapidity contribution

  ⇒ Integral of the function: Production cross sections

Experimental energy distributions

α distribution for Carbon target

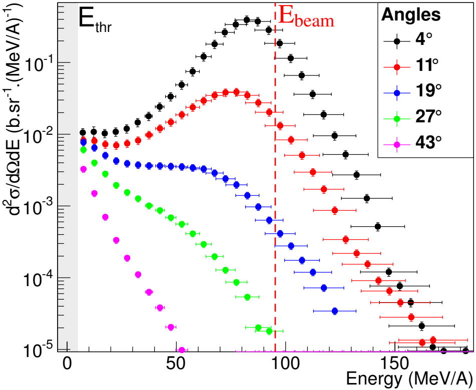

α distribution for all targets

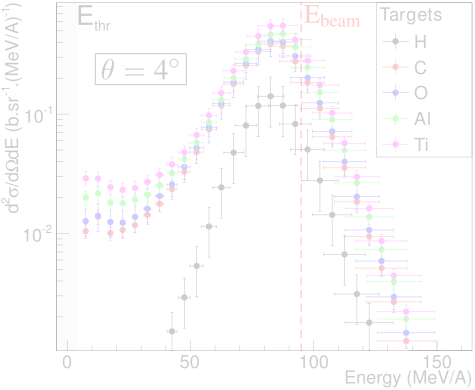

- Projectile fragmentation dominates at small angles $\rightarrow E_{mean} \approx E_{beam}$.
- $\partial^2\sigma/\partial\Omega\partial E$ increases with the target mass, especially at low energies.
- Only QP contribution (Z>1) for the hydrogen target.

Experimental energy distributions

α distribution for Carbon target

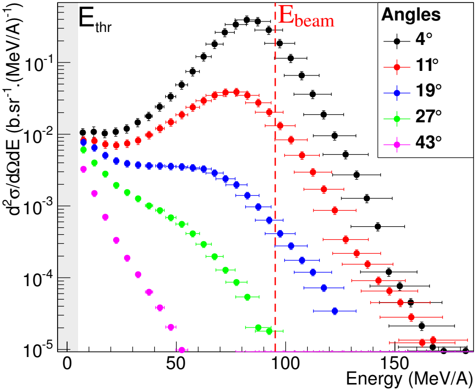

α distribution for all targets

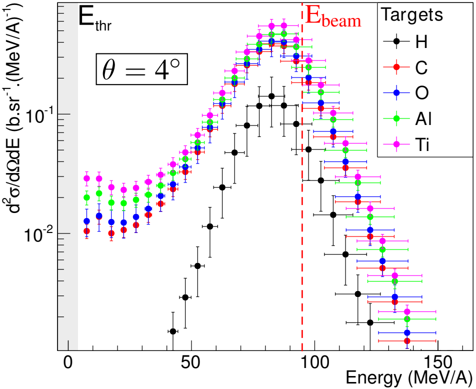

- Projectile fragmentation dominates at small angles $\rightarrow E_{mean} \approx E_{beam}$.
- $\partial^2\sigma/\partial\Omega\partial E$ increases with the target mass, especially at low energies.
- Only QP contribution (Z>1) for the hydrogen target.

Zero degree measurements

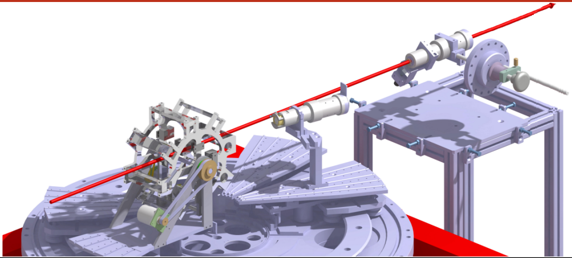

Zero degree measurements at GANIL (september 2013)

- Projectile: 95 MeV/A ^{12}C
- Thin targets: C, CH_2, Al and ^{nat}Ti
- 2 telescopes:
  - $\rightarrow$ 9° measurements $\Rightarrow$ E600 $\frac{d^2\sigma}{d\Omega dE}$ have been confirmed $\sim 3\%$.
  - $\rightarrow$ 0° measurements $\Rightarrow$ $d\sigma/d\Omega$ with $\sim$ 10-15 % accuracy.
    - $\Rightarrow$ $d\sigma/d\Omega$ for Z = 2 to Z = 5.
    - $\Rightarrow$ $d\sigma/d\Omega$ for ^4He, ^6Li, ^7Li, ^7Be, ^{10}B and ^{11}B isotopes.

Zero degree measurements

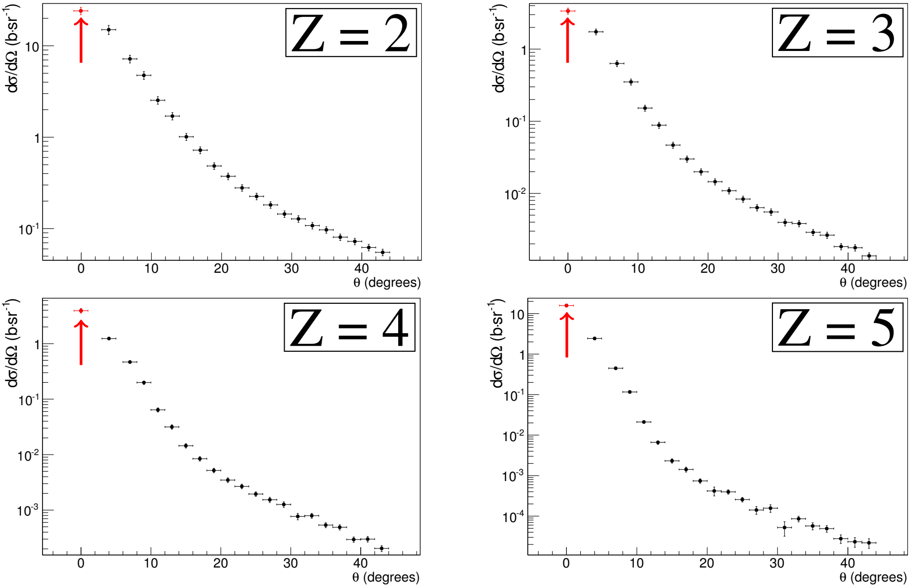

Angular distribution fits : Gaus + Exp -vs- Exp + Exp

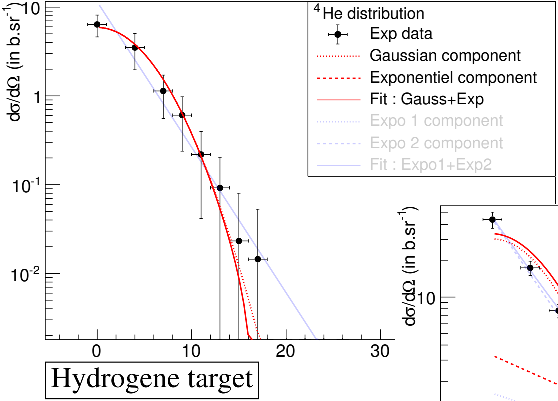

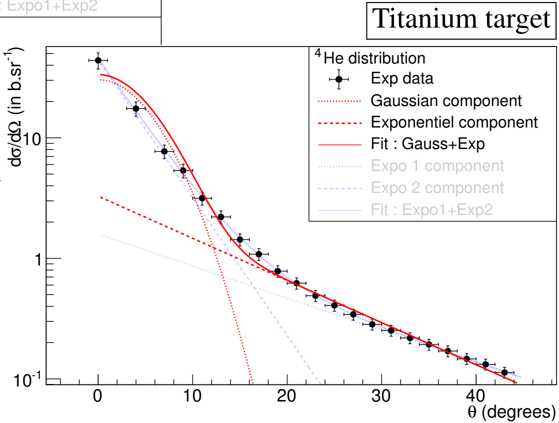

Angular distribution fits : Gaus + Exp -vs- Exp + Exp

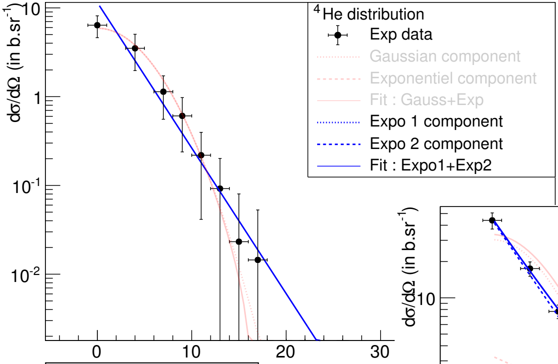

Hydrogene target

Titanium target

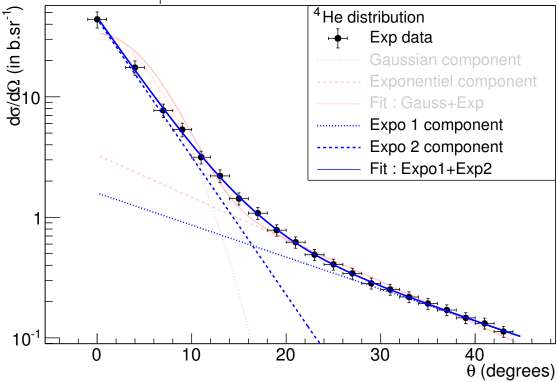

Angular distribution fits: Let's get crazy! Gaus + Exp + Exp

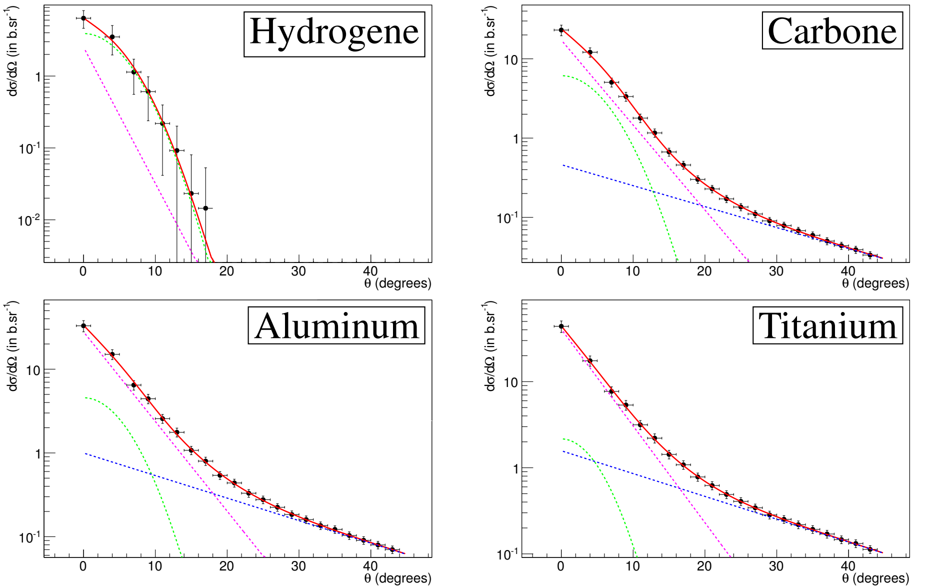

Angular distribution fits: Let's get crazy! Gaus + Exp + Exp

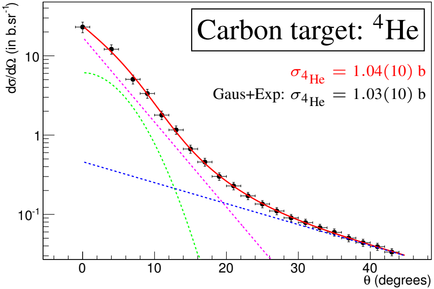

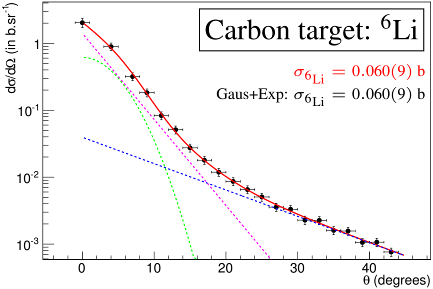

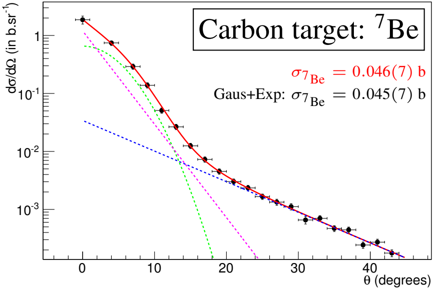

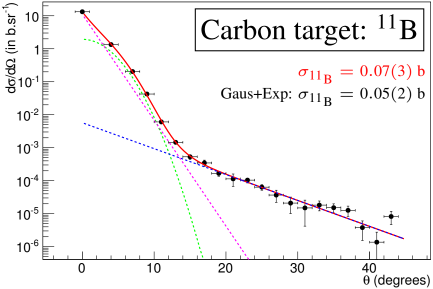

Angular distribution fits: Let's get crazy! Gaus + Exp + Exp

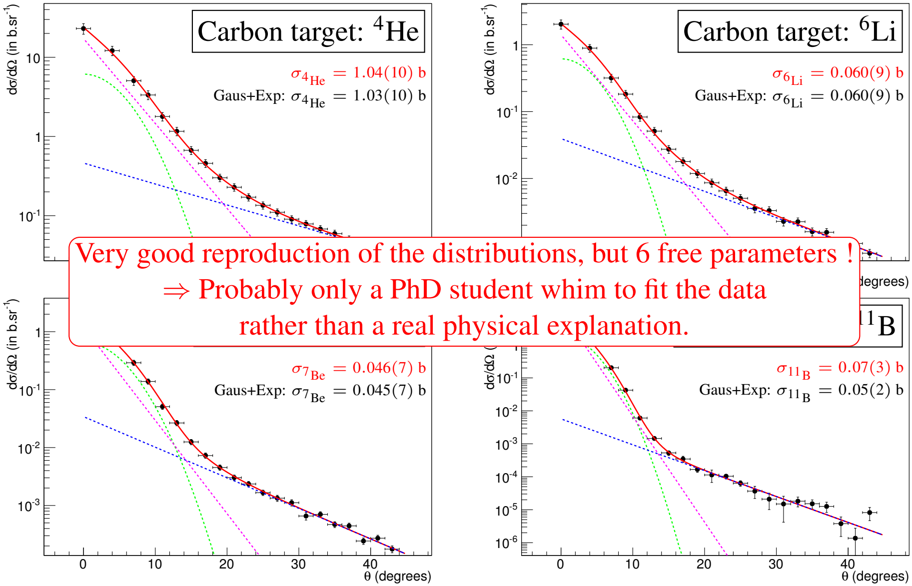

Very good reproduction of the distributions, but 6 free parameters !

$\Rightarrow$ Probably only a PhD student whim to fit the data rather than a real physical explanation.

PMMA reconstruction

Composite target cross sections reconstruction from cross sections of elemental targets:

$$\overbrace{\frac{d\sigma}{d\Omega}(C_5H_8O_2)}^{\text{Experimental PMMA target}} \stackrel{?}{=} \underbrace{5\times\frac{d\sigma}{d\Omega}(C)+8\times\frac{d\sigma}{d\Omega}(H)+2\times\frac{d\sigma}{d\Omega}(O)}_{\text{Calculated PMMA target}}$$

PMMA reconstruction

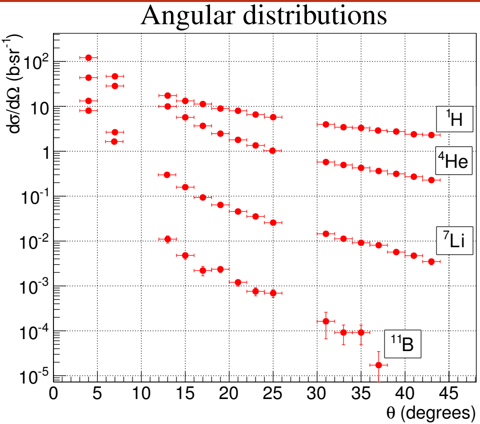

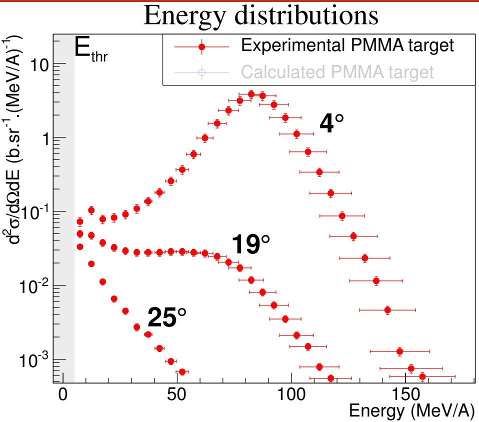

- Very good reconstruction of the experimental PMMA target cross sections by combining the H, C and O targets cross sections.

⟹ Cross sections can be deduced for almost all organic tissues.

PMMA reconstruction

Angular distributions

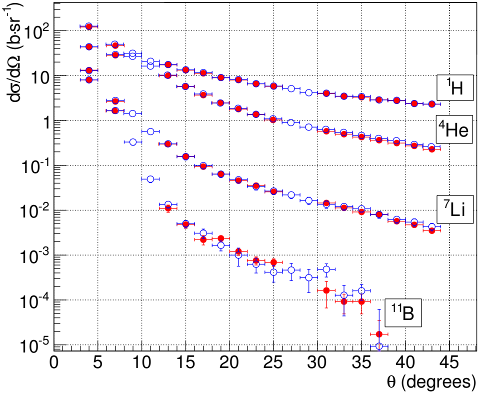

Energy distributions

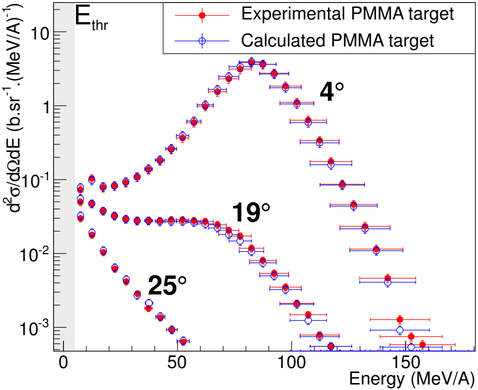

- Very good reconstruction of the experimental PMMA target cross sections by combining the H, C and O targets cross sections.

  ⟹ Cross sections can be deduced for almost all organic tissues.

Outlines

Geant4 simulations characteristics

Geant4 parametrization

Geant4 version	9.6-p01
Electromagnetic interactions	em standard option 3
Particle transport cuts	700 μm
Total nucleus-nucleus cross sections	Glauber-Gribov model: *"G4GGNuclNuclCrossSection"*
Dynamical part of the collision (Entrance Chanel model)	G4BinaryLightIonReaction (BIC) Q4QMDReaction (QMD) Intra Nuclear Cascade of Liège (INCL)
Statistical part of the collision (Exit Chanel model)	Generalized Evaporation model (GEM) Fermi Break Up (FBU)

Production rates (Carbon target)

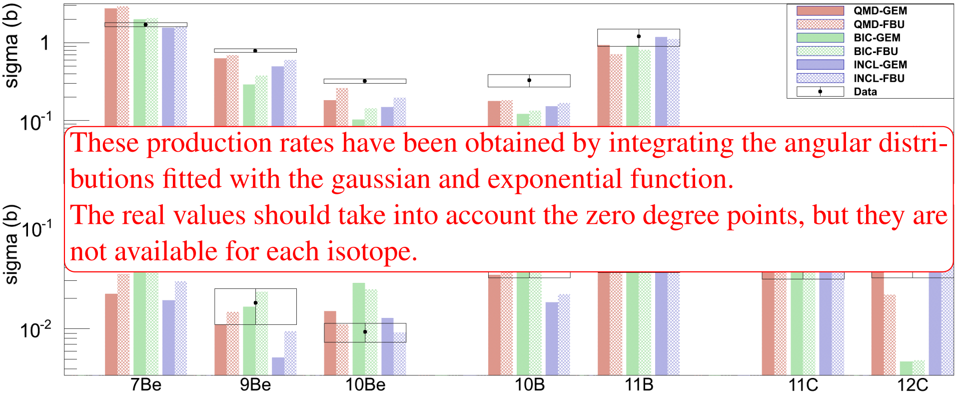

These production rates have been obtained by integrating the angular distributions fitted with the gaussian and exponential function.
The real values should take into account the zero degree points, but they are not available for each isotope.

⇒ None of these models is able to accurately reproduce the production rates.

- For more precise conclusions, a "χ^2" needs to be calculated:

$$\chi^2 = \sum_i \left(\frac{Y_i(\mathrm{G4}) - Y_i(\mathrm{Exp})}{\sigma(Y_i(\mathrm{Exp}))} \right)^2 \quad \text{with} \quad i = {}^1\mathrm{H}, {}^2\mathrm{H}, \ldots\ldots, {}^{11}\mathrm{C}, {}^{12}\mathrm{C}$$

Production rates (Carbon target)

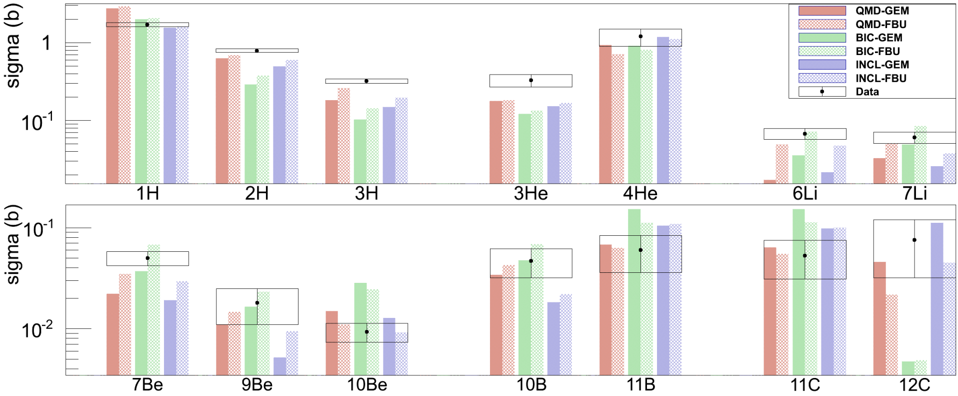

$\Rightarrow$ None of these models is able to accurately reproduce the production rates.

- For more precise conclusions, a "χ^2" needs to be calculated:

$$\chi^2 = \sum_i \left(\frac{Y_i(\mathrm{G4}) - Y_i(\mathrm{Exp})}{\sigma(Y_i(\mathrm{Exp}))} \right)^2 \quad \text{with} \quad i = {}^1\mathrm{H}, {}^2\mathrm{H}, \ldots\ldots, {}^{11}\mathrm{C}, {}^{12}\mathrm{C}$$

Production rates (Carbon target)

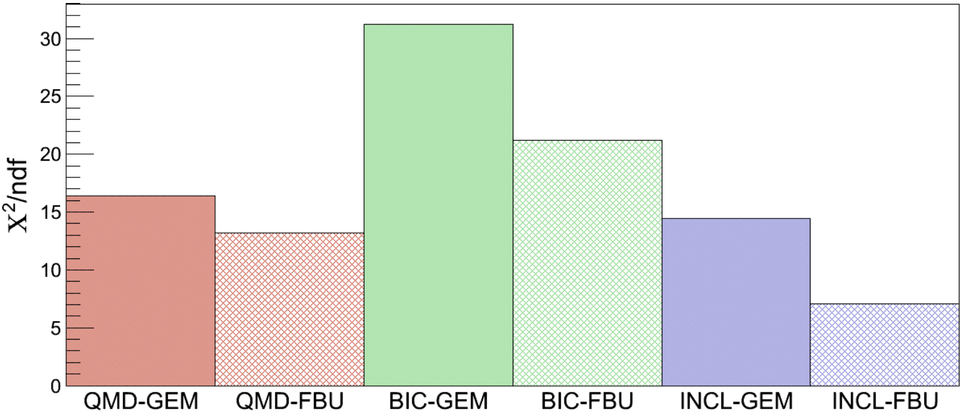

- INCL is the model which seems to best reproduce the production rates.
- The Fermi Break-up seems to give more predictive results.
  $\Rightarrow$ Only Fermi Break-up will be presented in the following.

Angular distributions (Carbon target)

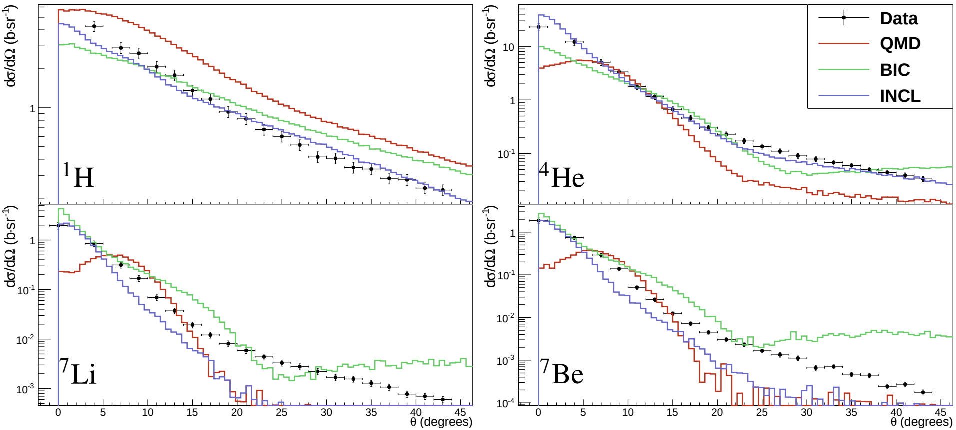

- QMD fails to reproduce the angular distributions.
- BIC is slightly better at forward angles but does not reproduce large angles.
- INCL gives better results for Z≤2, but only at forward angles for Z>2.

Angular distributions (Carbon target)

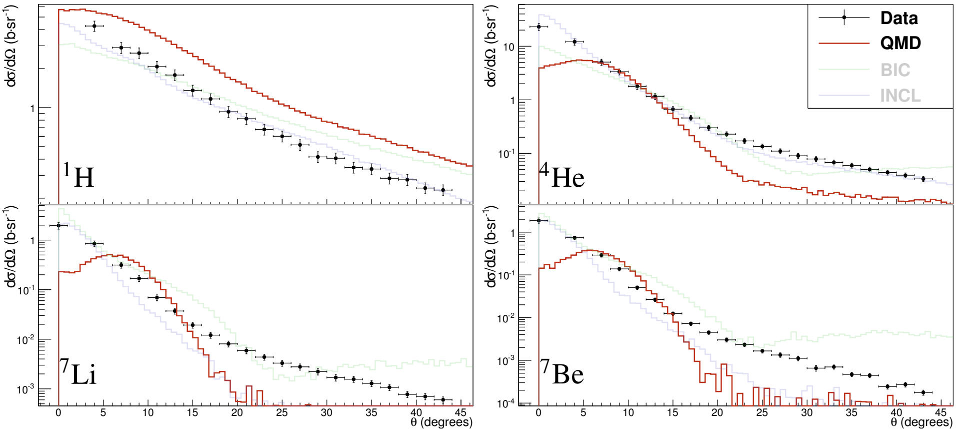

- QMD fails to reproduce the angular distributions.
- BIC is slightly better at forward angles but does not reproduce large angles.
- INCL gives better results for $Z \leq 2$, but only at forward angles for $Z > 2$.

Angular distributions (Carbon target)

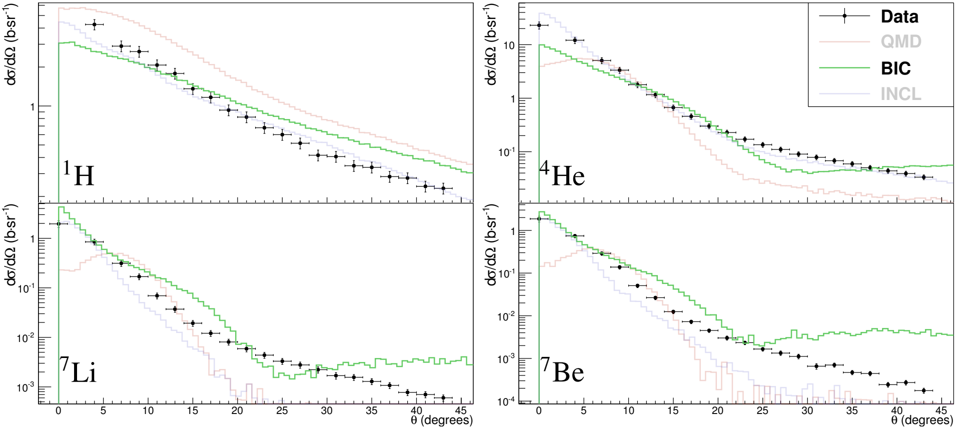

- QMD fails to reproduce the angular distributions.
- BIC is slightly better at forward angles but does not reproduce large angles.
- INCL gives better results for $Z \leq 2$, but only at forward angles for $Z > 2$.

Angular distributions (Carbon target)

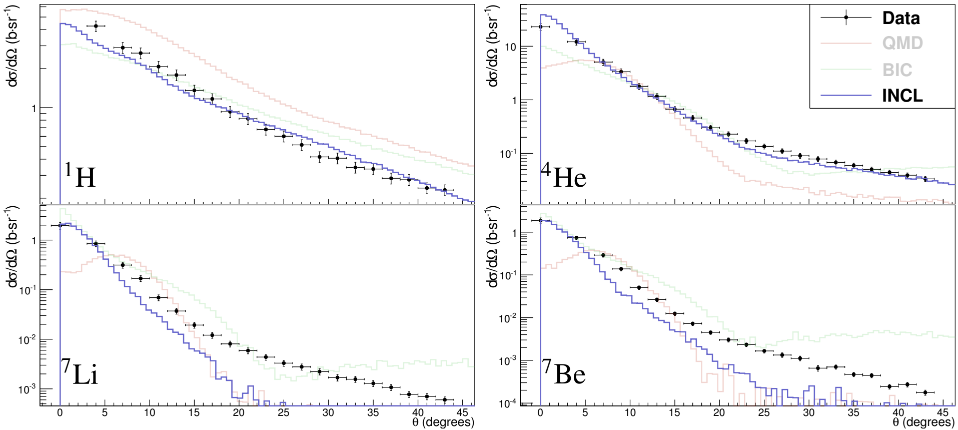

- QMD fails to reproduce the angular distributions.
- BIC is slightly better at forward angles but does not reproduce large angles.
- INCL gives better results for $Z \leq 2$, but only at forward angles for $Z > 2$.

What about the nucleon gaussian width in QMD

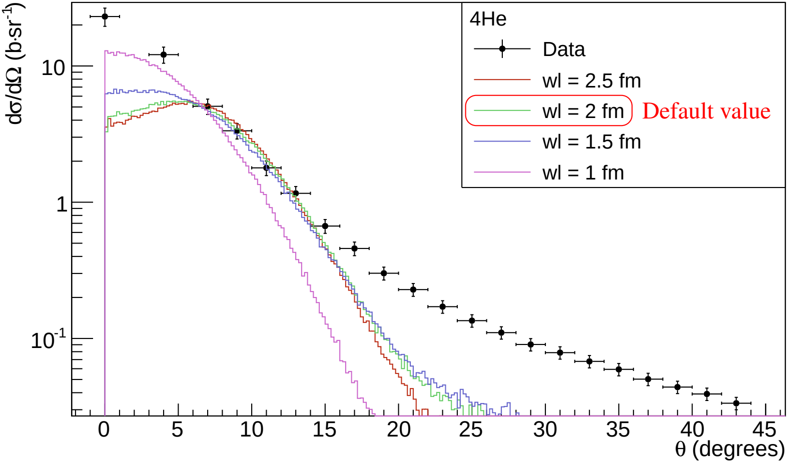

No magic solution!

⇒ The improvement on the small angles creates a larger disagreement for the large angles.

Energy distributions (Carbon target)

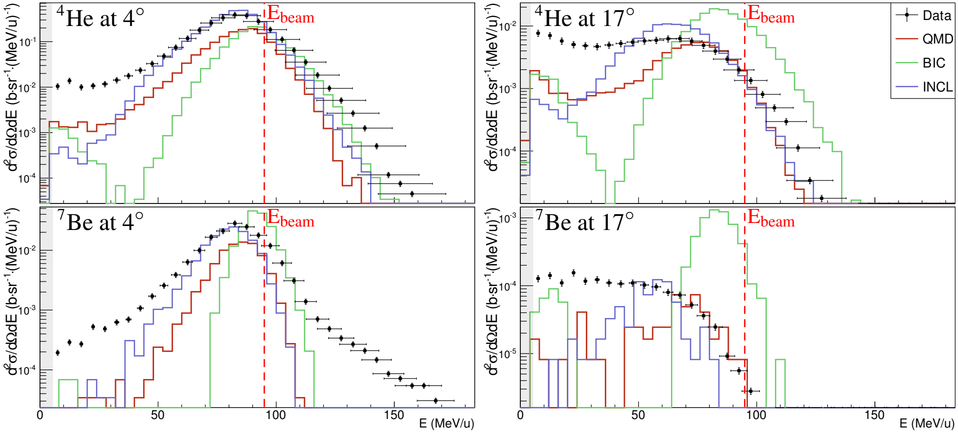

- BIC : Width too small, E mean too high, no mid-rapidity emission
- INCL: QP well reproduced, mid-rapidity shape not reproduced
- QMD: Best global shape but mid-rapidity still underestimated

Energy distributions (Carbon target)

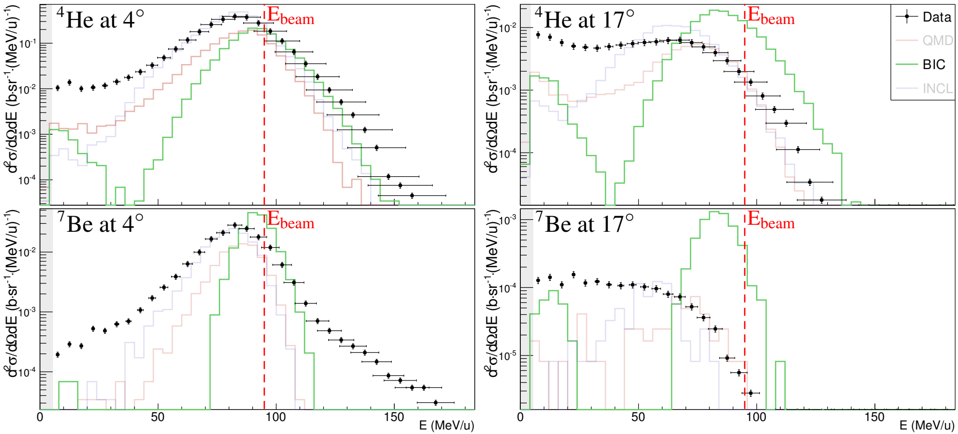

- BIC : Width too small, E mean too high, no mid-rapidity emission
- INCL: QP well reproduced, mid-rapidity shape not reproduced
- QMD: Best global shape but mid-rapidity still underestimated

Energy distributions (Carbon target)

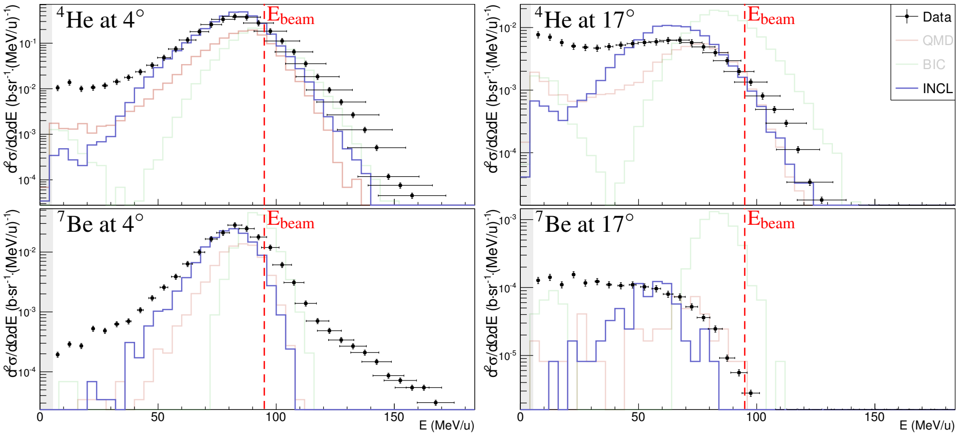

- BIC : Width too small, E mean too high, no mid-rapidity emission
- INCL: QP well reproduced, mid-rapidity shape not reproduced
- QMD: Best global shape but mid-rapidity still underestimated

Energy distributions (Carbon target)

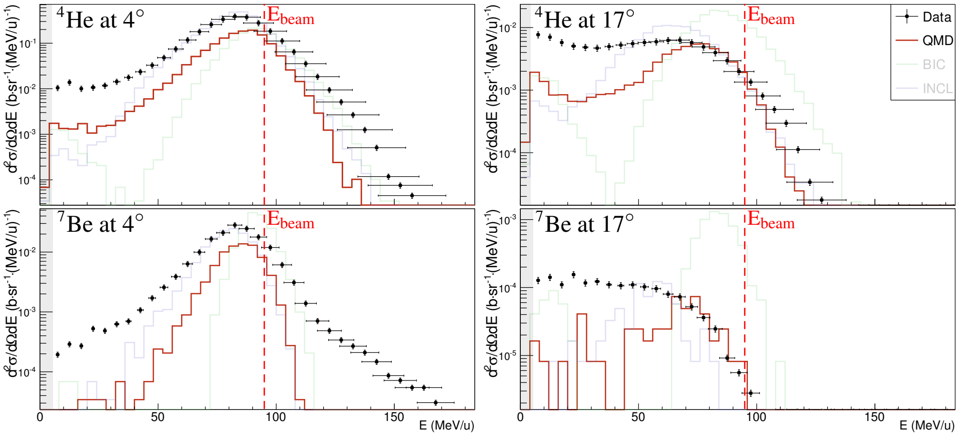

- BIC : Width too small, E mean too high, no mid-rapidity emission
- INCL: QP well reproduced, mid-rapidity shape not reproduced
- QMD: Best global shape but mid-rapidity still underestimated

Target comparisons (^{4}He production at 4°)

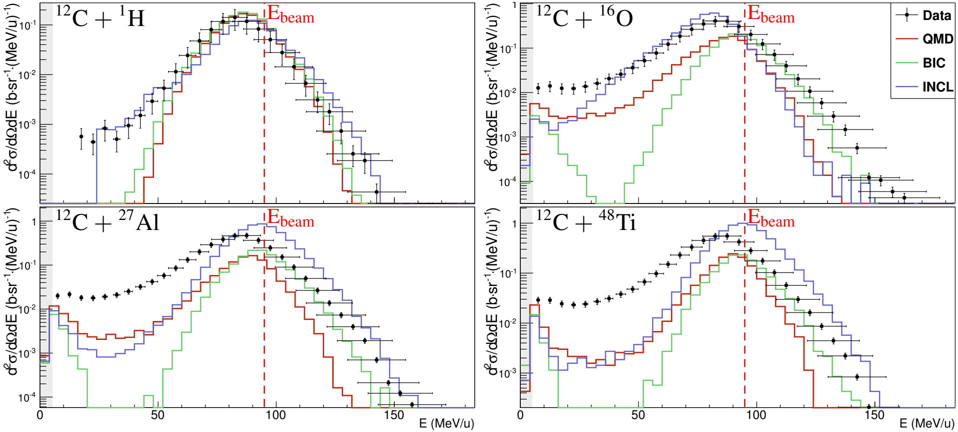

- Hydrogen target well reproduced by the three models, especially by INCL.
- The heavier the target, the larger the disagreement.
- Different behavior of INCL for ^{27}Al and ^{48}Ti targets $\Rightarrow$ kinematic inversion.

Outlines

The HIPSE model results

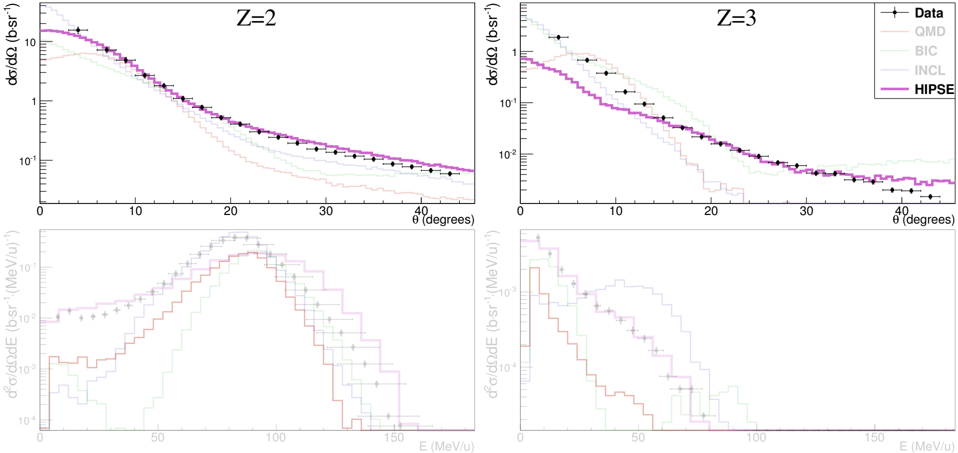

- QP poorly reproduced but mid-rapidity well described.
- The overlap region of the reaction needs to be taken into account to reproduce the mid-rapidity

The HIPSE model results

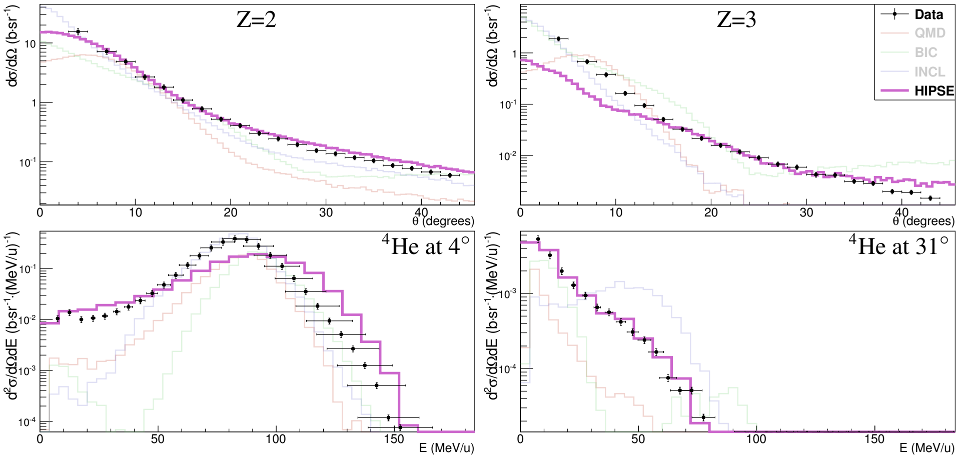

- QP poorly reproduced but mid-rapidity well described.
- The overlap region of the reaction needs to be taken into account to reproduce the mid-rapidity

Development of a new model

Nucleus initialization

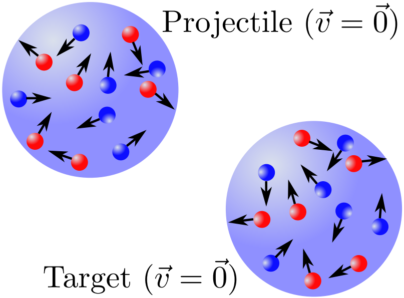

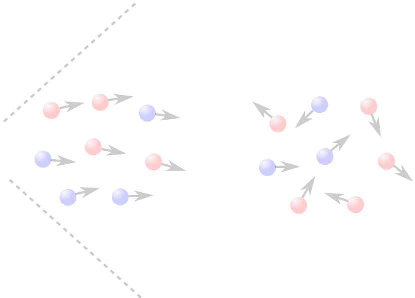

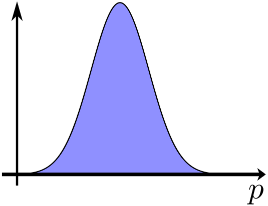

Nucleons momentum distribution from harmonic oscillator wave functions:

$$p(x) = \left[1 + \frac{(A-4) \times b_0 \times x^2}{6}\right] \times x^2 e^{-b_0 x^2}$$

Development of a new model

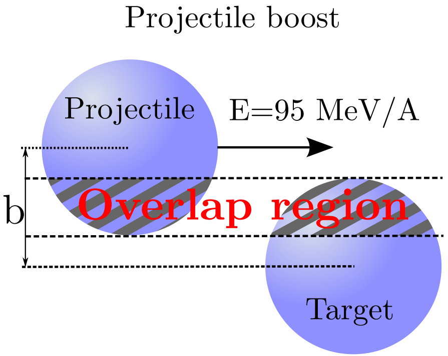

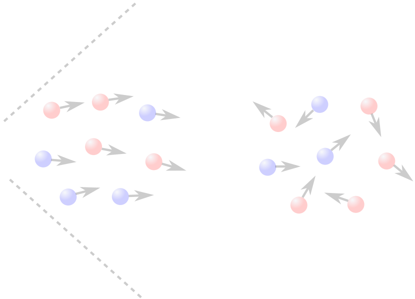

⇒ Projectile boost in the Lab frame

⇒ Calculation of the overlapping volume of the reaction

Development of a new model

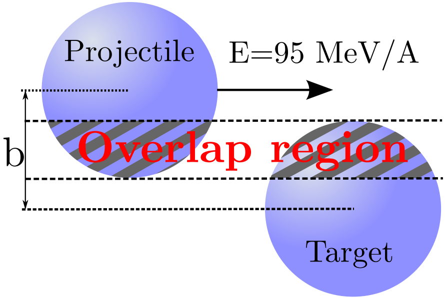

Overlapping nucleons

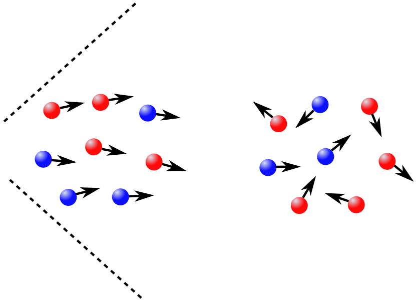

First parameter: Collision rate per nucleon

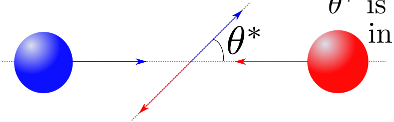

θ^* is randomly chosen in the CM frame

Best results for ~0.5 coll per nucleon

Development of a new model

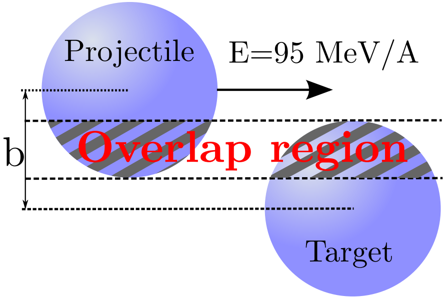

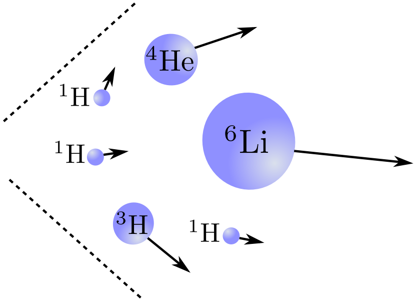

$\Rightarrow$Random coalescence in $\vec{p}$ space

$\Rightarrow$Second parameter: Cut on the mean energy of the fragments

$$\Rightarrow {}^A_Z\mathrm{X} \text{ is rejected if } \mathrm{E}_{mean} > 25 \text{ MeV}$$

$$\mathrm{E}_{mean} = \frac{1}{A} \times \sum_{i=1}^{A} E_i$$

Development of a new model

- The model is first scaled on the data at large angles and high energies.
  - ⇒ Only mid-rapidity contribution.
- The obtained scale factor is then applied:
  - ⇒ to the smaller angles,
  - ⇒ to the angular distributions.

^{4}He at 29°

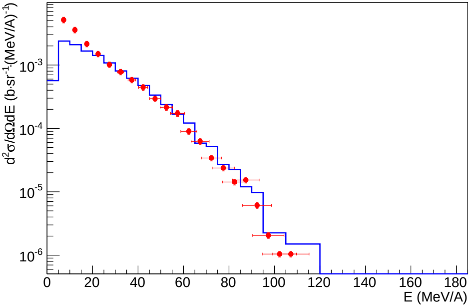

^{6}Li at 29°

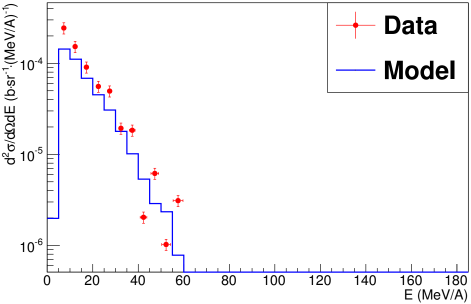

Preliminary results

Development of a new model

- The model is first scaled on the data at large angles and high energies.
  - ⇒ Only mid-rapidity contribution.
- The obtained scale factor is then applied:
  - ⇒ to the smaller angles,
  - ⇒ to the angular distributions.

^{4}He at 15°

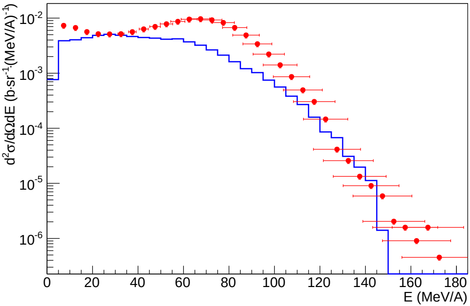

^{6}Li at 15°

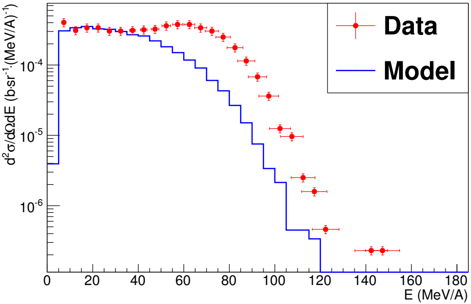

Preliminary results

Development of a new model

- The model is first scaled on the data at large angles and high energies.
  - ⇒ Only mid-rapidity contribution.
- The obtained scale factor is then applied:
  - ⇒ to the smaller angles,
  - ⇒ to the angular distributions.

^{4}He at 9°

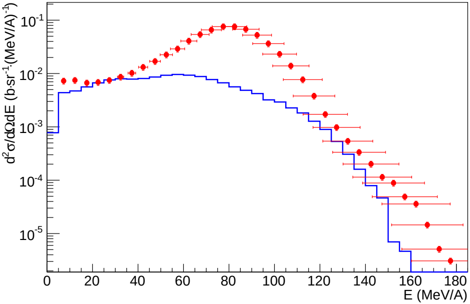

^{6}Li at 9°

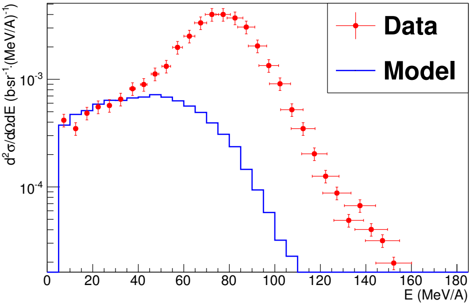

Preliminary results

Development of a new model

- The model is first scaled on the data at large angles and high energies.
  - ⇒ Only mid-rapidity contribution.
- The obtained scale factor is then applied:
  - ⇒ to the smaller angles,
  - ⇒ to the angular distributions.

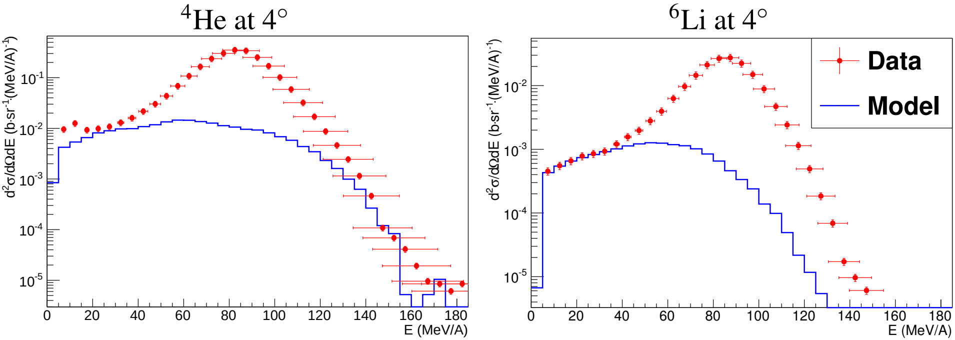

Preliminary results

Development of a new model

- The model is first scaled on the data at large angles and high energies.
  - $\Rightarrow$ Only mid-rapidity contribution.
- The obtained scale factor is then applied:
  - $\Rightarrow$ to the smaller angles,
  - $\Rightarrow$ to the angular distributions.

^{4}He at 4°

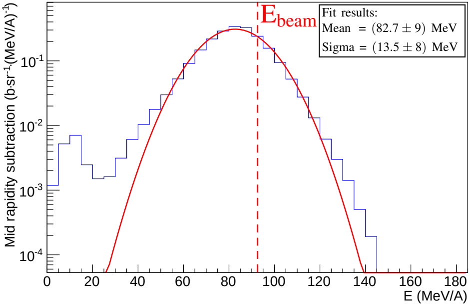

^{6}Li at 4°

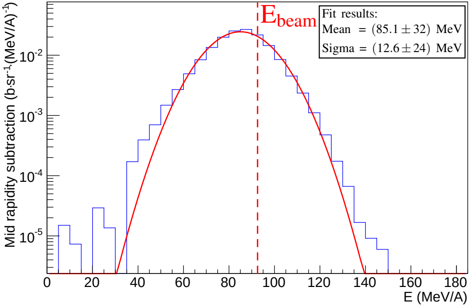

Preliminary results

Development of a new model

- The model is first scaled on the data at large angles and high energies.
  - $\Rightarrow$ Only mid-rapidity contribution.
- The obtained scale factor is then applied:
  - $\Rightarrow$ to the smaller angles,
  - $\Rightarrow$ to the angular distributions.

^{4}He angular distribution

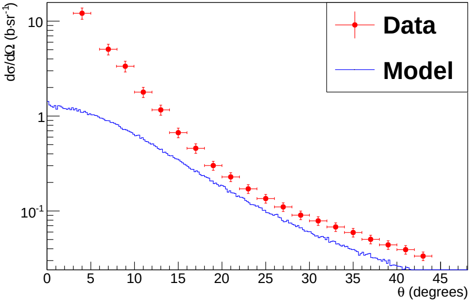

^{6}Li angular distribution

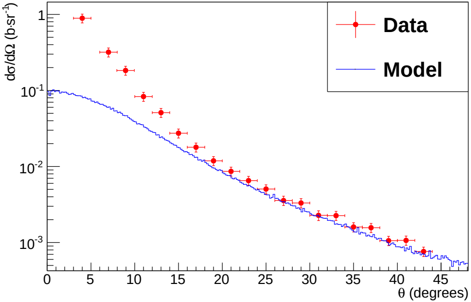

Preliminary results

Conclusions 1/2

Experimental conclusions

- Fragmentation cross sections of 95 MeV/A ^{12}C ions on thin targets (H, C, O, Al, Ti) have been measured in a first experiment at GANIL:
  - ⇒ Double differential cross sections $\partial^2\sigma/\partial E\partial\Omega$
  - ⇒ Angular differential cross sections from 4 to 43°
  - ⇒ Fragment production cross sections
- The zero degree cross sections have been measured in a second experiment:
  - ⇒ $\partial\sigma/\partial\Omega$ for Z=2 to Z=5.
  - ⇒ cross-checked with the first experiment at 9° (3% accuracy).
- Development of a quasi-automated analysis method based on the ROOT and KaliVeda toolkits.
- Systematic errors have been estimated/corrected (CsI light pulse shape analysis)
- Composite targets can be deduced from the cross sections of elemental targets (→ organic tissues)

Conclusions 1/2

Experimental conclusions

- Fragmentation cross sections of 95 MeV/A ^{12}C ions on thin targets (H, C, O, Al, Ti) have been measured in a first experiment at GANIL:
  - ⇒ Double differential cross sections $\partial^2\sigma/\partial E\partial\Omega$
  - ⇒ Angular differential cross sections from 4 to 43°
  - ⇒ Fragment production cross sections
- The zero degree cross sections have been measured in a second experiment:
  - ⇒ $\partial\sigma/\partial\Omega$ for Z=2 to Z=5.
  - ⇒ cross-checked with the first experiment at 9° (3% accuracy).
- Development of a quasi-automated analysis method based on the ROOT and KaliVeda toolkits.
- Systematic errors have been estimated/corrected (CsI light pulse shape analysis)
- Composite targets can be deduced from the cross sections of elemental targets (→ organic tissues)

Conclusions 1/2

Experimental conclusions

- Fragmentation cross sections of 95 MeV/A ^{12}C ions on thin targets (H, C, O, Al, Ti) have been measured in a first experiment at GANIL:
  - ⇒ Double differential cross sections $\partial^2\sigma/\partial E\partial\Omega$
  - ⇒ Angular differential cross sections from 4 to 43°
  - ⇒ Fragment production cross sections
- The zero degree cross sections have been measured in a second experiment:
  - ⇒ $\partial\sigma/\partial\Omega$ for Z=2 to Z=5.
  - ⇒ cross-checked with the first experiment at 9° (3% accuracy).
- Development of a quasi-automated analysis method based on the ROOT and KaliVeda toolkits.
- Systematic errors have been estimated/corrected (CsI light pulse shape analysis)
- Composite targets can be deduced from the cross sections of elemental targets ($\rightarrow$ organic tissues)

Conclusions 1/2

Experimental conclusions

- Fragmentation cross sections of 95 MeV/A ^{12}C ions on thin targets (H, C, O, Al, Ti) have been measured in a first experiment at GANIL:
  - ⇒ Double differential cross sections $\partial^2\sigma/\partial E\partial\Omega$
  - ⇒ Angular differential cross sections from 4 to 43°
  - ⇒ Fragment production cross sections
- The zero degree cross sections have been measured in a second experiment:
  - ⇒ $\partial\sigma/\partial\Omega$ for Z=2 to Z=5.
  - ⇒ cross-checked with the first experiment at 9° (3% accuracy).
- Development of a quasi-automated analysis method based on the ROOT and KaliVeda toolkits.
- Systematic errors have been estimated/corrected (CsI light pulse shape analysis)
- Composite targets can be deduced from the cross sections of elemental targets (→ organic tissues)

Conclusions 1/2

Experimental conclusions

- Fragmentation cross sections of 95 MeV/A ^{12}C ions on thin targets (H, C, O, Al, Ti) have been measured in a first experiment at GANIL:
  - $\Rightarrow$ Double differential cross sections $\partial^2\sigma/\partial E\partial\Omega$
  - $\Rightarrow$ Angular differential cross sections from 4 to 43°
  - $\Rightarrow$ Fragment production cross sections
- The zero degree cross sections have been measured in a second experiment:
  - $\Rightarrow$ $\partial\sigma/\partial\Omega$ for Z=2 to Z=5.
  - $\Rightarrow$ cross-checked with the first experiment at 9° (3% accuracy).
- Development of a quasi-automated analysis method based on the ROOT and KaliVeda toolkits.
- Systematic errors have been estimated/corrected (CsI light pulse shape analysis)
- Composite targets can be deduced from the cross sections of elemental targets ($\rightarrow$ organic tissues)

Conclusions 2/2

Simulations conclusions

- GEANT4 Monte Carlo simulations have shown that:
  - ⇒ The Fermi Break-Up seems to be the most predictive de-excitation model.
  - ⇒ The BIC model is the least capable to reproduce the data. It does not produce mid-rapidity particles and the QP energies are too high.
  - ⇒ The INCL model reproduces well the QP fragmentation for forward angles but the shape of the mid-rapidity contribution is not reproduced.
  - ⇒ The QMD model does not reproduce the angular distributions but is the model which best reproduces the global shape of the energy distributions, although the mid-rapidity is still underestimated.
- The HIPSE model has shown that the overlap region of the reaction needs to be taken into account to accurately reproduce the mid-rapidity emissions.
- The development of a simple model has shown that the mid-rapidity kinematic is compatible with a randomize coalescence in the momentum space

Conclusions 2/2

Simulations conclusions

- GEANT4 Monte Carlo simulations have shown that:
  - ⇒ The Fermi Break-Up seems to be the most predictive de-excitation model.
  - ⇒ The BIC model is the least capable to reproduce the data. It does not produce mid-rapidity particles and the QP energies are too high.
  - ⇒ The INCL model reproduces well the QP fragmentation for forward angles but the shape of the mid-rapidity contribution is not reproduced.
  - ⇒ The QMD model does not reproduce the angular distributions but is the model which best reproduces the global shape of the energy distributions, although the mid-rapidity is still underestimated.
- The HIPSE model has shown that the overlap region of the reaction needs to be taken into account to accurately reproduce the mid-rapidity emissions.
- The development of a simple model has shown that the mid-rapidity kinematic is compatible with a randomize coalescence in the momentum space

Conclusions 2/2

Simulations conclusions

- GEANT4 Monte Carlo simulations have shown that:
  - ⇒ The Fermi Break-Up seems to be the most predictive de-excitation model.
  - ⇒ The BIC model is the least capable to reproduce the data. It does not produce mid-rapidity particles and the QP energies are too high.
  - ⇒ The INCL model reproduces well the QP fragmentation for forward angles but the shape of the mid-rapidity contribution is not reproduced.
  - ⇒ The QMD model does not reproduce the angular distributions but is the model which best reproduces the global shape of the energy distributions, although the mid-rapidity is still underestimated.
- The HIPSE model has shown that the overlap region of the reaction needs to be taken into account to accurately reproduce the mid-rapidity emissions.
- The development of a simple model has shown that the mid-rapidity kinematic is compatible with a randomize coalescence in the momentum space

Conclusions 2/2

Simulations conclusions

- GEANT4 Monte Carlo simulations have shown that:
  - ⇒ The Fermi Break-Up seems to be the most predictive de-excitation model.
  - ⇒ The BIC model is the least capable to reproduce the data. It does not produce mid-rapidity particles and the QP energies are too high.
  - ⇒ The INCL model reproduces well the QP fragmentation for forward angles but the shape of the mid-rapidity contribution is not reproduced.
  - ⇒ The QMD model does not reproduce the angular distributions but is the model which best reproduces the global shape of the energy distributions, although the mid-rapidity is still underestimated.
- The HIPSE model has shown that the overlap region of the reaction needs to be taken into account to accurately reproduce the mid-rapidity emissions.
- The development of a simple model has shown that the mid-rapidity kinematic is compatible with a randomize coalescence in the momentum space

Conclusions 2/2

Simulations conclusions

- GEANT4 Monte Carlo simulations have shown that:
  - ⇒ The Fermi Break-Up seems to be the most predictive de-excitation model.
  - ⇒ The BIC model is the least capable to reproduce the data. It does not produce mid-rapidity particles and the QP energies are too high.
  - ⇒ The INCL model reproduces well the QP fragmentation for forward angles but the shape of the mid-rapidity contribution is not reproduced.
  - ⇒ The QMD model does not reproduce the angular distributions but is the model which best reproduces the global shape of the energy distributions, although the mid-rapidity is still underestimated.
- The HIPSE model has shown that the overlap region of the reaction needs to be taken into account to accurately reproduce the mid-rapidity emissions.
- The development of a simple model has shown that the mid-rapidity kinematic is compatible with a randomize coalescence in the momentum space

Conclusions 2/2

Simulations conclusions

- GEANT4 Monte Carlo simulations have shown that:
  - ⇒ The Fermi Break-Up seems to be the most predictive de-excitation model.
  - ⇒ The BIC model is the least capable to reproduce the data. It does not produce mid-rapidity particles and the QP energies are too high.
  - ⇒ The INCL model reproduces well the QP fragmentation for forward angles but the shape of the mid-rapidity contribution is not reproduced.
  - ⇒ The QMD model does not reproduce the angular distributions but is the model which best reproduces the global shape of the energy distributions, although the mid-rapidity is still underestimated.
- The HIPSE model has shown that the overlap region of the reaction needs to be taken into account to accurately reproduce the mid-rapidity emissions.
- The development of a simple model has shown that the mid-rapidity kinematic is compatible with a randomize coalescence in the momentum space

Conclusions 2/2

Simulations conclusions

- GEANT4 Monte Carlo simulations have shown that:
  - ⇒ The Fermi Break-Up seems to be the most predictive de-excitation model.
  - ⇒ The BIC model is the least capable to reproduce the data. It does not produce mid-rapidity particles and the QP energies are too high.
  - ⇒ The INCL model reproduces well the QP fragmentation for forward angles but the shape of the mid-rapidity contribution is not reproduced.
  - ⇒ The QMD model does not reproduce the angular distributions but is the model which best reproduces the global shape of the energy distributions, although the mid-rapidity is still underestimated.
- The HIPSE model has shown that the overlap region of the reaction needs to be taken into account to accurately reproduce the mid-rapidity emissions.
- The development of a simple model has shown that the mid-rapidity kinematic is compatible with a randomize coalescence in the momentum space

Outlooks

- In order to obtain more constraining data to improve nuclear models:
  - $\Rightarrow$ Measurements of ^{12}C fragmentation at 50 MeV/A have been proposed at GANIL for 2015 (France Hadron beam time).
  - $\Rightarrow$ A new resource center for hadrontherapy, the ARCHADE center, is expected in Caen in 2019 $\rightarrow$ measurements with different beams (α to ^{12}C) up to 400 MeV/A.
- Improvement of the proposed model to obtain the entire kinematic (QP+QT+MR) and production yields.

The data and the experimental setup details are available with free access at:
`http://hadrontherapy-data.in2p3.fr`

E600 analysis method	: J. Dudouet *et al.*, Nucl. Instrum. Methods A 715, 98 (2013)
Systematic errors and data	: J. Dudouet *et al.*, Phys. Rev. C 88, 024606 (2013)
Comparisons with simulations:	J. Dudouet *et al.*, arXiv:1309.1544, submitted to Phys. Med. Biol.

Thank you for your attention!

Telescope analysis: Energy calibration

- Development of an algorithm to simplify the analysis. By building an identification grid for each telescope, the algorithm will process:
  - ⇒ the energy calibration,
  - ⇒ the particle identification.

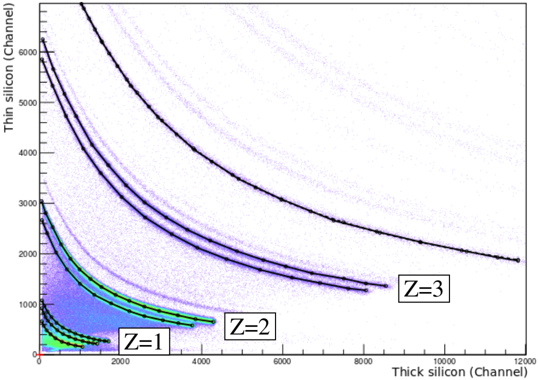

J. Dudouet *et al.*, Nucl. Instrum. Methods A 715, 98 (2013)

Telescope analysis: Energy calibration

Functional describing the energy loss ΔE in a detector as a function of the residual energy E deposited in a second detector in which the particle has stopped:

$$\Delta E = \left[(gE)^{\mu+\nu+1} + (\lambda Z^{\alpha} A^{\beta})^{\mu+\nu+1} + \xi Z^2 A^{\mu} (gE)^{\nu}\right]^{\frac{1}{\mu+\nu+1}} - gE$$

where $g, \mu, \nu, \lambda, \alpha, \beta, \xi$ are fitting parameters.

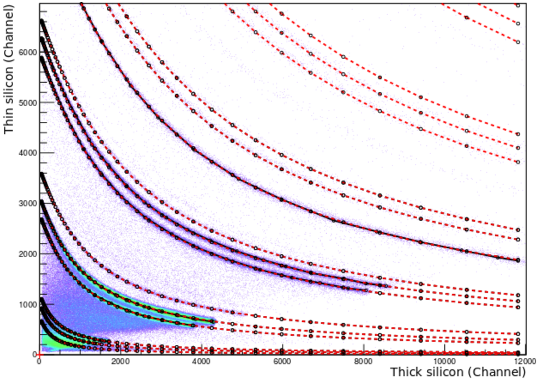

J. Dudouet *et al.*, Nucl. Instrum. Methods A 715, 98 (2013)

Telescope analysis: Energy calibration

Functional describing the energy loss ΔE in a detector as a function of the residual energy E deposited in a second detector in which the particle has stopped:

$$\Delta E = \left[(gE)^{\mu+\nu+1} + (\lambda Z^{\alpha} A^{\beta})^{\mu+\nu+1} + \xi Z^2 A^{\mu} (gE)^{\nu}\right]^{\frac{1}{\mu+\nu+1}} - gE$$

where $g, \mu, \nu, \lambda, \alpha, \beta, \xi$ are fitting parameters.

Experimental grid (Channel)

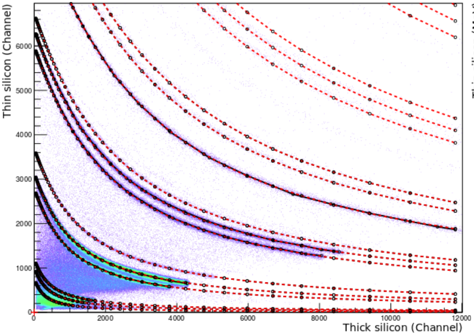

Theoretical grid (MeV)

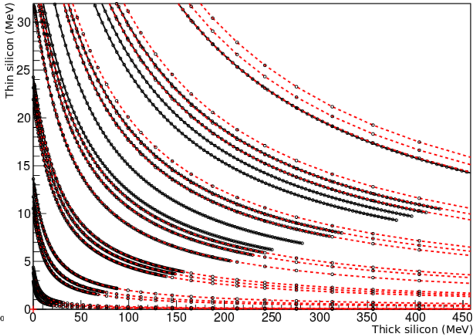

J. Dudouet *et al.*, Nucl. Instrum. Methods A 715, 98 (2013)

Telescope analysis: Energy calibration

- The energy calibration of the silicon detectors is simplified and very accurate.
- The energy calibration of the CsI crystals is then deduced from the thick silicon energy calibration.

Energy calibration of the silicon detectors:

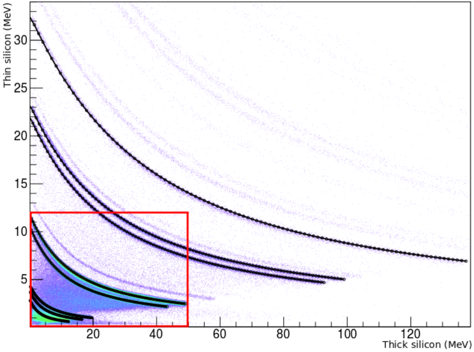

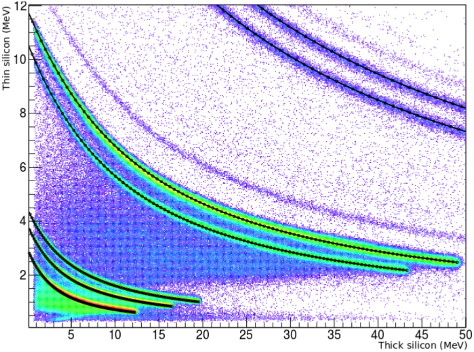

J. Dudouet *et al.*, Nucl. Instrum. Methods A 715, 98 (2013)

Telescope analysis: Energy calibration

Energy calibration of the CsI crystals

- CsI calibration using the silicon calibration:
  - ⇒ Analytic expression of $E_{\text{Thick silicon}} = f(E_{\text{CsI}})$
  - ⇒ Thick silicon energy calibration
  - ⇒ Residual energy deduced from energy loss calculations

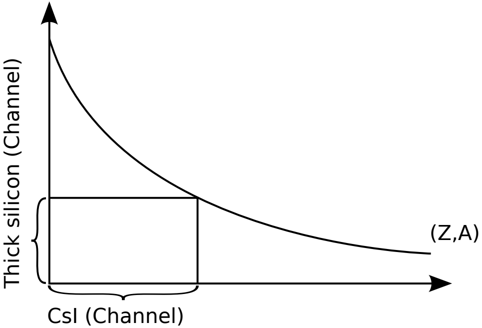

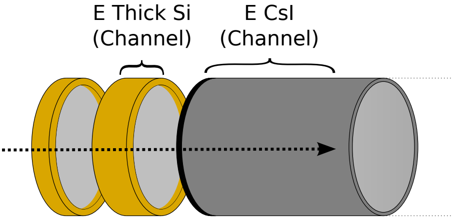

Telescope analysis: Energy calibration

Energy calibration of the CsI crystals

- CsI calibration using the silicon calibration:
  - ⇒ Analytic expression of $E_{\text{Thick silicon}} = f(E_{\text{CsI}})$
  - ⇒ Thick silicon energy calibration
  - ⇒ Residual energy deduced from energy loss calculations

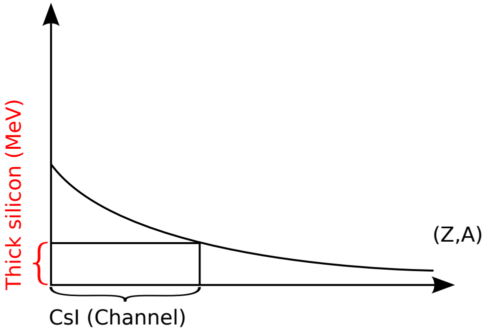

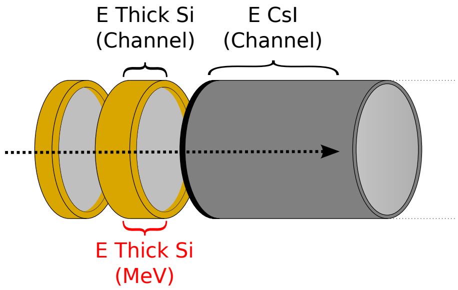

Telescope analysis: Energy calibration

Energy calibration of the CsI crystals

- CsI calibration using the silicon calibration:
  - ⇒ Analytic expression of $E_{\text{Thick silicon}} = f(E_{\text{CsI}})$
  - ⇒ Thick silicon energy calibration
  - ⇒ Residual energy deduced from energy loss calculations

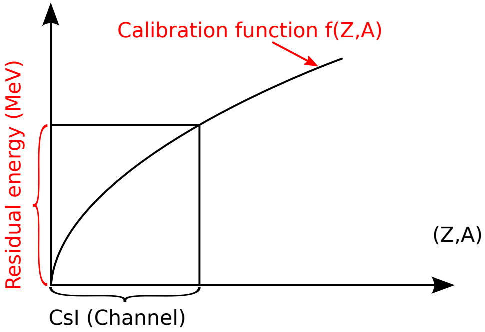

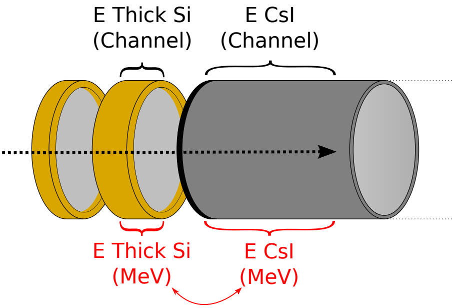

Telescope analysis: Particle identification

- From the identification grids previously described:
  - ⇒ The charge and mass of each event is determined
  - ⇒ A PID value is calculated as: $PID = Z + 0.1 \times (A_{real} - 2Z)$

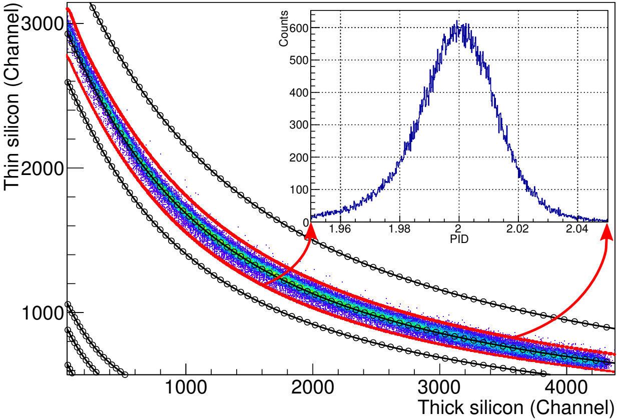

J. Dudouet *et al.*, Nucl. Instrum. Methods A 715, 98 (2013)

Telescope analysis: Particle identification

- From the identification grids previously described:
  - ⇒ The charge and mass of each event is determined
  - ⇒ A PID value is calculated as: $PID = Z + 0.1 \times (A_{real} - 2Z)$

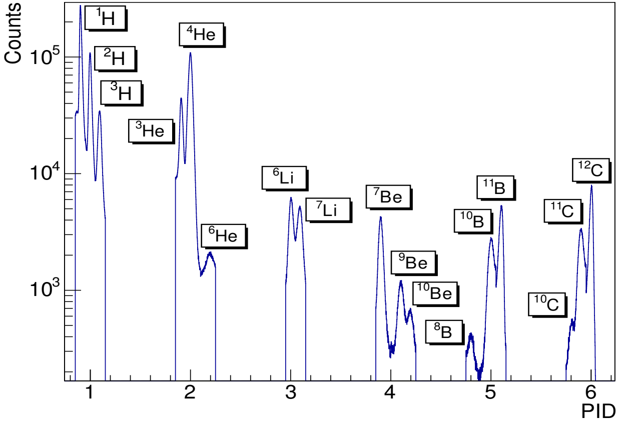

J. Dudouet *et al.*, Nucl. Instrum. Methods A 715, 98 (2013)

A short INCL description

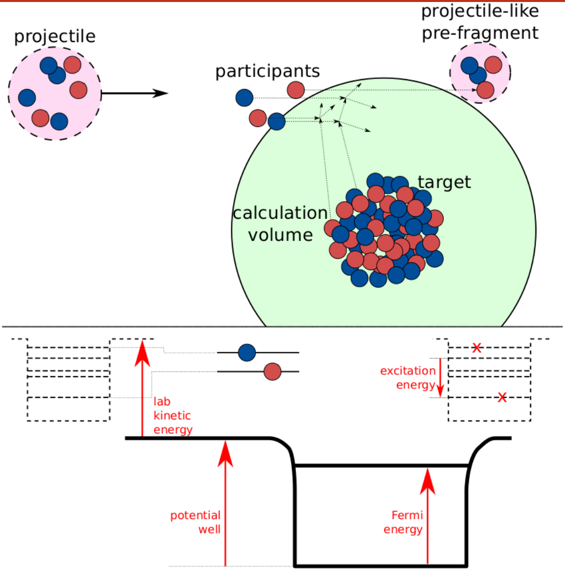

B. Braunn *et al.*, J. Physics: Conf. Series 420, 012163 (2013)

INCL better reproduces the target fragmentation. The default parametrization implemented in GEANT4, called "accurate projectile mode" uses inverse kinematics:

- $^{12}\mathrm{C} \to {}^{1}\mathrm{H} \Rightarrow {}^{1}\mathrm{H} \to {}^{12}\mathrm{C}$
- $^{12}\mathrm{C} \to {}^{12}\mathrm{C} \Rightarrow {}^{12}\mathrm{C} \to {}^{12}\mathrm{C}$
- $^{12}\mathrm{C} \to {}^{16}\mathrm{O} \Rightarrow {}^{16}\mathrm{O} \to {}^{12}\mathrm{C}$

But INCL cannot use projectile heavier than A=18, direct kinematics are then used:

- $^{12}\mathrm{C} \to {}^{27}\mathrm{Al} \Rightarrow {}^{12}\mathrm{C} \to {}^{27}\mathrm{Al}$
- $^{12}\mathrm{C} \to {}^{48}\mathrm{Ti} \Rightarrow {}^{12}\mathrm{C} \to {}^{48}\mathrm{Ti}$

If both target and projectile masses are above 18, the Binary Cascade is used.